

Synthetic GPCRs for programmable sensing and control of cell behaviour

<https://doi.org/10.1038/s41586-024-08282-3>

Received: 28 February 2024

Accepted: 24 October 2024

Published online: 04 December 2024

Open access

 Check for updates

Nicholas A. Kalogriopoulos^{1,9}, Reika Tei^{1,9}, Yuqi Yan², Peter M. Klein³, Matthew Ravalin¹, Bo Cai¹, Ivan Soltész³, Yulong Li^{2,4} & Alice Ting^{1,5,6,7,8}✉

Synthetic receptors that mediate antigen-dependent cell responses are transforming therapeutics, drug discovery and basic research^{1,2}. However, established technologies such as chimeric antigen receptors³ can only detect immobilized antigens, have limited output scope and lack built-in drug control^{3–7}. Here we engineer synthetic G-protein-coupled receptors (GPCRs) that are capable of driving a wide range of native or non-native cellular processes in response to a user-defined antigen. We achieve modular antigen gating by engineering and fusing a conditional auto-inhibitory domain onto GPCR scaffolds. Antigen binding to a fused nanobody relieves auto-inhibition and enables receptor activation by drug, thus generating programmable antigen-gated G-protein-coupled engineered receptors (PAGERS). We create PAGERS that are responsive to more than a dozen biologically and therapeutically important soluble and cell-surface antigens in a single step from corresponding nanobody binders. Different PAGER scaffolds allow antigen binding to drive transgene expression, real-time fluorescence or endogenous G-protein activation, enabling control of diverse cellular functions. We demonstrate multiple applications of PAGER, including induction of T cell migration along a soluble antigen gradient, control of macrophage differentiation, secretion of therapeutic antibodies and inhibition of neuronal activity in mouse brain slices. Owing to its modular design and generalizability, we expect PAGERS to have broad utility in discovery and translational science.

Cell-surface receptors sense specific extracellular cues, transmit those signals across the cell membrane and convert them into defined cellular responses. Engineering modular synthetic receptors that can recapitulate this transmembrane signalling is a key challenge for reprogramming cell behaviour. Synthetic receptors derived from T cell receptors (chimeric antigen receptors³) and the Notch receptor⁴ have enabled diverse applications in medicine⁵ and basic research². However, these platforms are limited by their inherent mechanisms of activation (antigen-induced clustering and force, respectively), which restrict both antigen and output scope. GPCRs, the largest and most diverse family of cell-surface receptors, could offer a more flexible scaffold for programming cellular responses with synthetic receptors. GPCRs are seven-transmembrane cell-surface receptors that mediate responses to diverse extracellular signals, including hormones, neurotransmitters, peptides, light, force and odorants. Ligand binding induces a conformational change in the GPCR that, in turn, activates heterotrimeric G proteins and downstream intracellular signalling cascades.

The challenge in harnessing GPCRs for synthetic receptor technology is that they are not structurally modular proteins. Previous efforts to alter their ligand specificity have required labour-intensive structure-guided mutagenesis^{8,9} and directed evolution^{10,11}. To enable

straightforward and modular antigen gating, we engineered a conditional auto-inhibitory domain for GPCR scaffolds. We fused a nanobody and a receptor auto-inhibitory domain to the extracellular N terminus of the GPCR such that binding of the auto-inhibitory domain to the GPCR and binding of the nanobody to an antigen are mutually exclusive. Thus, antigen binding relieves auto-inhibition and enables receptor activation by an agonist (Fig. 1a). Once activated, PAGER can drive diverse native or synthetic outputs, including transgene expression (PAGER_{TF}), endogenous G-protein activation (PAGER_G) or real-time fluorescence (PAGER_{FL}).

When selecting the optimal GPCR for the PAGER scaffold, we considered two requirements: (1) it should be activatable by a bioorthogonal small-molecule agonist; and (2) it should be sensitive to the activity of a genetically encodable antagonist that can be fused to the GPCR. We focused on DREADDs^{9,11,12} (designer receptors exclusively activated by designer drugs), GPCRs that have been engineered to be insensitive to native ligands but activatable by highly selective drug-like small molecules with minimal activity on endogenous receptors.

We started from the κ -opioid receptor DREADD (κ ORD), owing to the established activity of peptide antagonists for its parent κ -opioid receptor^{9,13} (κ OR). To read out PAGER activation using a transcriptional

¹Department of Genetics, Stanford University, Stanford, CA, USA. ²Peking-Tsinghua Center for Life Sciences, Academy for Advanced Interdisciplinary Studies, Peking University, Beijing, China.

³Department of Neurosurgery, Stanford University, Stanford, CA, USA. ⁴State Key Laboratory of Membrane Biology, New Cornerstone Science Laboratory, School of Life Sciences, Peking University, Beijing, China. ⁵Department of Biology, Stanford University, Stanford, CA, USA. ⁶Department of Chemistry, Stanford University, Stanford, CA, USA. ⁷Chan Zuckerberg Biohub—San Francisco, San Francisco, CA, USA. ⁸Phil & Penny Knight Initiative for Brain Resilience at the Wu Tsai Neurosciences Institute, Stanford University, Stanford, CA, USA. ⁹These authors contributed equally: Nicholas A. Kalogriopoulos, Reika Tei. ✉e-mail: ayting@stanford.edu

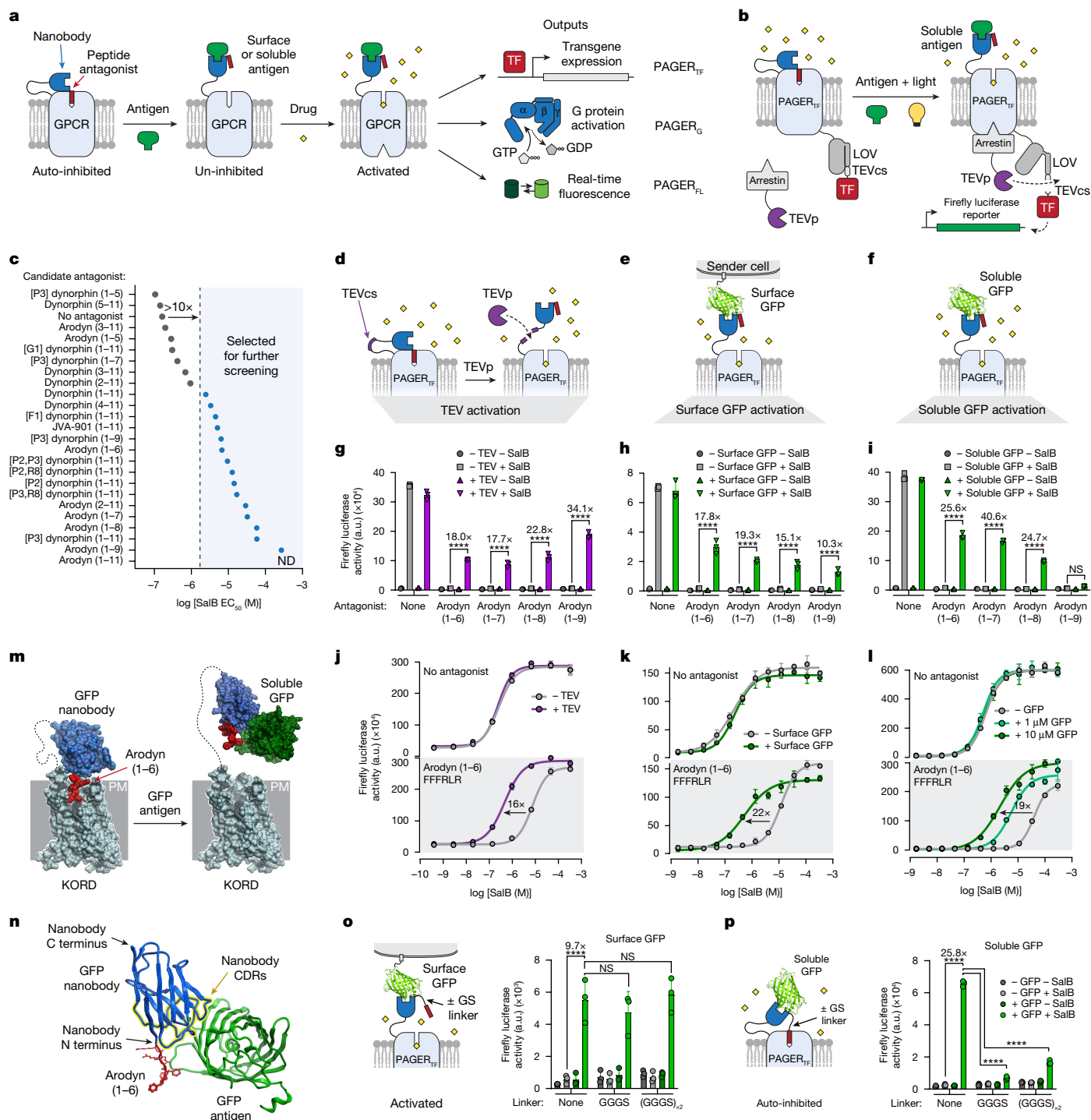


Fig. 1 | Design and optimization of PAGER. **a**, PAGER overview. Auto-inhibition by fused peptide antagonist is relieved by antigen binding and allows drug activation of the GPCR. PAGER activation can drive transgene expression (PAGER_{TF}), G-protein activation (PAGER_G) or real-time fluorescence (PAGER_{FL}). TF, transcription factor. **b**, Schematic of PAGER_{TF}. PAGER-driven transgene expression based on SPARK^{14,15} (specific protein association tool giving result transcriptional readout with rapid kinetics). PAGER_{TF} activation results in proteolytic release of a tethered transcription factor. LOV, light, oxygen- and voltage-sensitive domain. **c**, Summary of SalB EC₅₀ values for candidate antagonist peptides screened in PAGER_{TF}. *n* = 3 independent experiments, 3 replicates per condition. ND, not defined. **d–f**, Schematics for PAGER_{TF} activation by extracellular TEVp (**d**), surface-expressed GFP (**e**) or soluble GFP (**f**). **g–i**, PAGER_{TF} activity in response to SalB and TEV treatment (**g**), co-plating with HEK cells presenting surface GFP (**h**) or soluble GFP (**i**). *n* = 3, 5 or 4 independent experiments, respectively, 3 replicates per condition. Data are mean ± s.d. Two-way ANOVA with Tukey’s multiple comparisons test. **j–l**, SalB dose–response curves for PAGER_{TF} activity with arodyn (1–6) antagonist and TEV pretreatment (**j**), co-plating with HEK cells presenting surface GFP (**k**) or soluble GFP (**l**). *n* = 5, 2 or 2 independent experiments, respectively, 3 replicates per condition. Data are mean ± s.d. **m**, AlphaFold2 model of antagonist and antigen-dependent relief of antagonism in PAGER. PM, plasma membrane. **n**, AlphaFold2 model highlighting proximity between the CDRs (yellow) and N terminus of the nanobody, where the antagonist peptide (red) is fused. **o**, PAGER_{TF} variants with flexible Gly-Ser linkers can be activated by surface GFP expressed on co-plated HEK 293T cells. *n* = 3 independent experiments, 3 replicates per condition. Data are mean ± s.d. (two-way ANOVA with Tukey’s multiple comparisons test). **p**, PAGER_{TF} variants with flexible Gly-Ser linkers cannot be activated by soluble GFP. *n* = 3 independent experiments, 3 replicates per condition. Data are mean ± s.d. Two-way ANOVA with Tukey’s multiple comparisons test. **P* < 0.05, ***P* < 0.01, ****P* < 0.001, *****P* < 0.0001; NS, not significant.

reporter, we fused a transcription factor to κ ORD via a light-gated protease-sensitive linker, and co-expressed an arrestin-TEV protease (TEVp) fusion^{14,15} (PAGER_{TF}) (Extended Data Fig. 1a). PAGER_{TF} activation triggers arrestin-TEVp recruitment, and if light or furimazine are also present, then the tethered transcription factor will be released by proteolysis, translocate to the nucleus and drive reporter gene expression (Fig. 1b and Extended Data Fig. 1b,c). κ ORD-based PAGER_{TF} was optimized to produce robust expression of a firefly luciferase reporter in response to its small-molecule agonist salvinorin B (SalB) (Extended Data Fig. 1d-f).

We then screened a library of antagonist peptides to auto-inhibit PAGER_{TF}. The natural agonist of κ OR, dynorphin, is a 17-amino-acid peptide that binds with its N-terminal end buried in the orthosteric site of κ OR¹³ (Extended Data Fig. 1g). We selected 24 candidate antagonists based on mutated or truncated variants of dynorphin (sequences in Extended Data Fig. 1h) and fused them to the extracellular N-terminal end of κ ORD, separated by a GFP-specific nanobody (LaG17) and a TEVp cleavage site (TEVcs) (Extended Data Fig. 1i). To ensure efficient cell-surface targeting, all constructs were cloned after an IL-2 signal peptide, which leaves no N-terminal 'scar' that could interfere with antagonist function. Sixteen out of 24 peptides displayed antagonism in the context of PAGER_{TF} by shifting the half-maximal effective concentration (EC₅₀) of the SalB response more than tenfold (Fig. 1c; full dose-response curves in Supplementary Fig. 1).

Additionally, for PAGER to function as designed, the peptide antagonism must be reversible. To screen the 16 antagonized constructs for this property, we used extracellular recombinant TEVp to cleave off the antagonist and relieve antagonism (Fig. 1d). We found that all 16 constructs were reversibly antagonized—protease treatment re-sensitized PAGER_{TF} to SalB (Extended Data Fig. 2). We selected four constructs that use the dynorphin analogue arodyn¹⁶ for auto-inhibition, owing to their high signal-to-noise ratio in PAGER_{TF} (Fig. 1g,j and Supplementary Fig. 2).

With these activatable PAGER_{TF} constructs, we next tested for the ability of GFP antigen to relieve auto-inhibition and provide robust SalB activation. We performed this test in two separate assays: (1) with surface-expressed GFP introduced via co-culture (Fig. 1e,h,k and Extended Data Figs. 2a); and (2) with soluble recombinant GFP (Fig. 1f,i,l and Extended Data Fig. 2b). All anti-GFP PAGER_{TF} constructs responded in varying degrees to both surface-expressed and soluble GFP. We observed that longer arodyn peptides were better antagonists but were also more difficult to remove with GFP antigen, probably owing to higher affinity for the receptor. For this reason, we selected the shorter arodyn (1-6) peptide, which displayed sufficient antagonism and the greatest response to GFP, for all PAGER_{TF} constructs going forward.

PAGER was designed so that antigen binding sterically occludes the peptide antagonist, preventing it from occupying the orthosteric site; un-inhibited receptor can then be activated by drug (Fig. 1m). We hypothesized that this mechanism is enabled by the proximity between the antigen-binding loops (complementarity-determining regions (CDRs) 1-3) and N-terminal end of the nanobody, where the peptide antagonist is fused (Fig. 1n). This steric activation mechanism should operate for both cell-surface and soluble antigens. With cell-surface antigens however, tensile force between PAGER and the target antigen due to cell-cell contact and endocytosis could also displace the auto-inhibitory domain. To probe the mechanism of PAGER, we varied the linker length between the N terminus of the nanobody and the fused peptide antagonist by inserting one or two copies of a flexible GGGS linker. We hypothesized that flexible linkers might relieve steric occlusion of the antagonist by bound antigen and render PAGER insensitive to soluble antigens. Surface antigens, however, should still be able to activate PAGER using tensile force. Indeed, when including GS linkers between the nanobody and peptide antagonist, anti-GFP PAGER_{TF} could still be activated by surface GFP antigen (Fig. 1o), but its response to soluble GFP antigen was largely abrogated (Fig. 1p).

PAGER can sense and respond to diverse antigens

If PAGER is modular as designed, simply swapping the antigen-binding nanobody for a nanobody that binds a different antigen should produce a functional receptor that can sense and respond to the new antigen. To test the modularity of PAGER, we first replaced the nanobody in anti-GFP PAGER_{TF} with ten other GFP nanobodies and six mCherry nanobodies. These nanobodies bind to diverse epitopes on the surface of GFP and mCherry and should produce different spatial relationships between bound antigen and fused antagonist peptide. We first screened the constructs for expression, auto-inhibition and relief of auto-inhibition by TEVp treatment (Supplementary Fig. 3). All but two anti-GFP PAGER_{TF} constructs passed this initial screen. The remaining nine anti-GFP PAGER_{TF} and all six anti-mCherry PAGER_{TF} constructs showed strong activation in response to soluble recombinant GFP and mCherry, respectively (Extended Data Fig. 3a and Supplementary Fig. 4). The best anti-GFP PAGER_{TF} (containing LaG2 nanobody) could detect soluble GFP down to 1.5 nM, consistent with the published dissociation constant (K_d) of LaG2¹⁷ (16–19 nM), whereas the best anti-mCherry PAGER_{TF} (containing LaM8 nanobody) could detect 100 nM mCherry protein (Extended Data Fig. 3b). Neither PAGER was responsive to the other fluorescent protein, illustrating the high specificity of these synthetic receptors.

We used our panel of anti-GFP and anti-mCherry PAGER_{TF} constructs to examine the relationship between nanobody affinity and PAGER reversibility—that is, the time it takes after antigen washout for PAGER_{TF} to become non-responsive to agonist. PAGER_{TF} containing high-affinity nanobodies such as LaG2¹⁷ ($K_d = 16-19$ nM) or LaM6¹⁷ ($K_d = 0.26$ nM) continued to be activated by SalB, even 30 min after antigen washout. PAGER_{TF} containing the lower-affinity nanobodies LaG17¹⁷ ($K_d = 50$ nM) and LaM8¹⁷ ($K_d = 63$ nM) were unresponsive to SalB immediately following antigen washout (Extended Data Fig. 3c,d). Thus the reversibility and ability of PAGER_{TF} to function as a coincidence detector are largely controlled by the affinity of the nanobody.

We next attempted to generate PAGER_{TF} constructs for different antigens of various types, sizes and folds—including growth factors, cytokines, chemokines, receptor tyrosine kinases, other cancer-expressed surface receptors, a viral protein and a protease—by replacing the nanobody in PAGER_{TF} with nanobodies to each new antigen of interest. In this way, we created PAGER_{TF} for VEGF, HGF, TNF, IL-17, IL-23, soluble IL-6 receptor (sIL-6R), CCL2, EGFR, HER2, CD38, PD-L1, SARS-CoV-2 spike protein and urokinase-type plasminogen activator (uPA) (Fig. 2a, Extended Data Fig. 4 and Supplementary Fig. 5). Each PAGER was responsive to its cognate antigen, but non-responsive to mismatched antigens (Extended Data Fig. 5a).

Many nanobodies have been engineered against the receptor-binding domain (RBD) of SARS-CoV-2 spike protein in order to block binding to the ACE2 receptor and viral entry into cells¹⁸. We made PAGER_{TF} constructs using five different nanobodies that bind to RBD epitopes that are accessible in trimeric spike protein. All but one produced spike-responsive PAGER_{TF} (Extended Data Fig. 5b,c), further illustrating the modularity and generalizability of PAGER.

To apply PAGER_{TF}, we used it to build sense-and-respond synthetic circuits specifically for coupling antigen detection to the secretion of bioactive molecules. In one circuit (Fig. 2b), PAGER_{TF} expressed in HEK 293T cells was used to detect antigens associated with M2-type anti-inflammatory macrophages: VEGF, which can induce M2 polarization¹⁹, and CCL2²⁰ and PD-L1²¹, which are present in tumours associated with M2 macrophages. Upon detection of these antigens, activated PAGER_{TF} induced the production and secretion of IFN γ , which acted on co-cultured RAW 264.7 macrophages to convert them to an M1 pro-inflammatory state. Upregulation of the M1 markers CD86 and NOS2 was observed in antigen and SalB-treated samples, but not in negative controls (Fig. 2c). In addition, M1 conversion was evident in images of macrophage morphology (Fig. 2d and Extended Data Fig. 6).

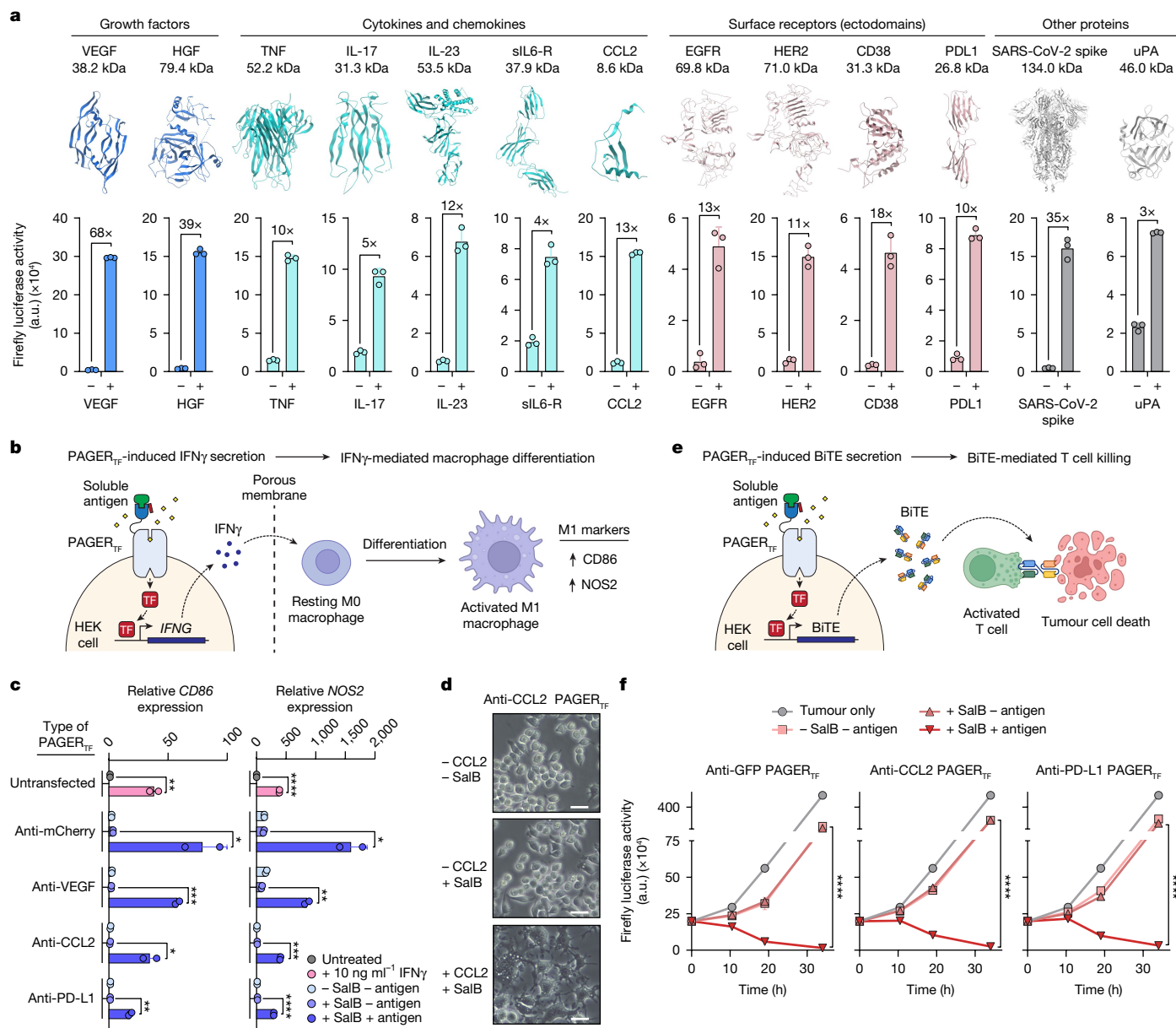


Fig. 2 | PAGER_{TF} can detect a wide variety of antigens. **a**, Top, ribbon structures of proteins sensed by PAGER_{TF}. Bottom, bar graphs of PAGER_{TF} activity in response to cognate antigen. Antigen and SalB concentrations are reported in Methods. For anti-VEGF, anti-TNF, anti-IL-17 and anti-uPA PAGERS, $n = 3$ independent experiments, 3 replicates per condition. For all other PAGERS, $n = 2$ independent experiments, 3 replicates per condition. Data are mean \pm s.d. Two-tailed Student's t -test. **b**, Schematic of PAGER_{TF}-driven macrophage differentiation in co-culture. PAGER_{TF} activation in HEK293T cells induces the secretion of mouse IFN γ which passes through a porous membrane and stimulates M1 macrophage differentiation. **c**, Relative expression of M1 macrophage markers *CD86* and *NOS2* in co-cultured RAW 264.7 macrophages, determined by quantitative PCR (qPCR). $n = 3$ experiments, 2 replicates per condition. Data are mean \pm s.d.

Two-tailed Student's t -test. **d**, Representative images of RAW 264.7 macrophages after 48 h of co-culture with anti-CCL2 PAGER_{TF}-IFN γ expressing HEK293T cells. Images are representative of $n = 3$ experiments. Representative macrophage images for the other PAGER_{TF} constructs in **c** can be found in Extended Data Fig. 6. Scale bars, 20 μ m. **e**, Schematic of PAGER_{TF}-driven BiTE-mediated T cell killing in co-culture. PAGER_{TF} activation in HEK293T cells induces the secretion of an anti-CD3/CD19 BiTE, which stimulates T cell recognition and killing of Nalm6 tumour cells. Firefly luciferase stably expressed in the Nalm6 cells is used to quantify live Nalm6 tumour cells. **f**, Time course of Nalm6 tumour cell survival in response to PAGER_{TF} activation by GFP, CCL2 or PD-L1. $n = 2$ experiments, 3 replicates per condition. Data are mean \pm s.d. Two-tailed Student's t -test.

These results show the potential of PAGER_{TF} for shifting cell identities in heterogeneous populations.

In a second synthetic circuit (Fig. 2e), we used PAGER_{TF} in HEK 293T cells to drive the secretion of a therapeutic antibody in response to tumour antigens. Bispecific T cell engagers (BiTEs) are bispecific antibodies that recruit T cells to tumour cells to drive tumour cell killing²². We used PAGER_{TF} to sense the tumour antigens CCL2²³ or PD-L1²⁴ (or GFP as a control) and respond by secreting an anti-CD3/CD19 BiTE, which increased the killing of co-cultured CD19-expressing Nalm6 tumour cells

by primary T cells (Fig. 2f). Collectively, these data demonstrate that PAGER_{TF} can drive biologically diverse and important cellular responses.

Antigen-dependent G-protein activation via PAGER

In PAGER_{TF}, antigen recognition drives transgene expression. For other applications, it may be desirable for antigen recognition to instead modulate endogenous signalling pathways. Because PAGER is based on GPCRs, we explored whether this platform could convert antigen

recognition into rapid activation of endogenous G-protein pathways and thereby drive diverse alterations in cell behaviour.

To explore this concept, we returned to the palette of DREADDs¹², which include engineered muscarinic acetylcholine receptors (M1–M5) that activate G_{α_q} (M1, M3 and M5) or G_{α_i} (M2 and M4)¹¹. In addition, chimeric DREADDs that activate G_{α_s} or $G_{\alpha_{12}}$ have been developed from M3 DREADD^{25,26}. These receptors no longer bind to acetylcholine (their endogenous ligand), but are activated by the orthogonal drugs clozapine *N*-oxide¹¹ (CNO) and deschloroclozapine²⁷ (DCZ). Although muscarinic GPCRs do not have known peptide antagonists, muscarinic toxin (MT) proteins from *Dendroaspis* snakes (Extended Data Fig. 7a) can antagonize specific muscarinic receptor subtypes^{28,29}. Thus, we explored the use of MT proteins for auto-inhibition of $PAGER_C$ constructs.

Starting from M1(G_q) and M4(G_i) DREADDs, we fused a GFP-specific nanobody and one of six possible MTs to their N-terminal ends. A TEVcs was inserted between the nanobody and DREADD to enable testing for reversible auto-inhibition. To measure $PAGER$ -driven G_q or G_i activation, we used the bioluminescence resonance energy transfer (BRET)-based TRUPATH assay³⁰ (Extended Data Fig. 7b). We found that MT1 on M1 DREADD produced the greatest fold change in G_q recruitment with TEVp treatment, indicating strong and reversible inhibition, whereas MT3 was the best toxin for gating M4 DREADD (Extended Data Fig. 7c and Supplementary Fig. 6). We recapitulated these findings in a different assay using luciferase gene expression as readout; the combinations of MT1–hM1Dq and MT3–hM4Di again yielded the greatest difference in luminescence with or without GFP (Extended Data Fig. 7d,e).

None of the MT proteins that we screened auto-inhibited the M3 DREADD (Extended Data Fig. 7c and Supplementary Fig. 6), preventing us from building $PAGER_{G_s}$ or $PAGER_{G_{12}}$ from the chimeric M3-based G_s ²⁵ and G_{12} ²⁶ DREADDs. However, owing to the high sequence and structural homology between M1 and M3, we could build similar chimeras using M1 instead of M3 to create $PAGER_{G_s}$ and $PAGER_{G_{12}}$ (Extended Data Figs. 7c and 8a and Supplementary Fig. 6). All $PAGER_C$ constructs were well-localized to the plasma membrane (Extended Data Fig. 8b).

With our panel of optimized $PAGER_{G_q}$, $PAGER_{G_s}$, $PAGER_{G_i}$ and $PAGER_{G_{12}}$ constructs, we performed a series of assays to test their coupling to endogenous G-protein pathways (Fig. 3a–d). First, we used western blotting to show antigen and CNO-dependent stimulation of ERK phosphorylation, a conserved downstream response to G-protein activation (Fig. 3e–h). Second, we used the TRUPATH assay to confirm antigen and DCZ-dependent activation of the corresponding G-protein partner for each $PAGER_C$ (Fig. 3i–l and Extended Data Fig. 8c–e). Third, we used fluorescent reporters to image second messengers specific to each G-protein pathway. For anti-GFP $PAGER_{G_q}$, we detected relocation of a fluorescent diacylglycerol (DAG) lipid-binding protein³¹ to the plasma membrane 30–60 s after $PAGER$ activation by antigen and DCZ (Extended Data Fig. 9a–c). These kinetics are consistent with the known timescale of phospholipase C-mediated DAG production at the plasma membrane, downstream of G_q activation³¹. We also used the Ca^{2+} indicator GCaMP6s³² to image mCherry and DCZ-dependent increases in cytosolic Ca^{2+} driven by anti-mCherry $PAGER_{G_q}$ (Fig. 3m and Extended Data Fig. 9d–e,j).

For $PAGER_{G_s}$ and $PAGER_{G_i}$, we used a fluorescent indicator of cAMP (G-Flamp2³³), which increases in response to stimulatory G_s and decreases in response to inhibitory G_i . In HEK cells expressing G-Flamp2³³ and either anti-mCherry $PAGER_{G_s}$ or anti-mCherry $PAGER_{G_i}$, we could observe mCherry-dependent increases (Fig. 3n and Extended Data Fig. 9f,g,k) or decreases (Fig. 3o and Extended Data Fig. 9h,i,l) in cAMP.

To test the antigen modularity of $PAGER_C$, we replaced the mCherry nanobody in $PAGER_{G_q}$ with a TNF nanobody (ozoralizumab³⁴; $K_d = 20.2$ pM) or VEGF scFv (brolucizumab³⁵; $K_d = 28.4$ pM). The resulting constructs elicited G_q activation in the presence of cognate antigens as measured by phospho-ERK and TRUPATH assays (Fig. 3p–s). TNF is an important pro-inflammatory cytokine that is released by macrophages during host defence³⁶. Our dose titration showed that anti-TNF $PAGER_{G_q}$ could

respond to TNF concentrations as low as 2 nM. VEGF is released by tumour cells, macrophages and platelets during angiogenesis and inflammation³⁷. Anti-VEGF $PAGER_{G_q}$ could detect 0.2 nM VEGF, a lower concentration than is released during idiopathic myelofibrosis, for example³⁸ (1–85 nM).

Finally, we studied the mechanism of $PAGER_C$ activation. For both anti-GFP $PAGER_{G_q}$ and anti-GFP $PAGER_{G_i}$, reducing the affinity of MT to the receptor resulted in increased binding of GFP to $PAGER$, indicating that MT intramolecular binding to receptor competes sterically with antigen binding to nanobody (Fig. 3t and Extended Data Fig. 10a,b). Moreover, GFP nanobodies with higher reported affinity were better overall at competing with MTs (Extended Data Fig. 10c) and they elicited better GFP-dependent activation of $PAGER_{G_q}$ (Extended Data Fig. 10d). Notably, truncation of MT or extending the linker between MT and nanobody by even a few amino acids resulted in lack of antagonism or loss of antigen-dependent activation, respectively (Extended Data Fig. 10e). As with $PAGER_{TF}$, the reversibility and ability of $PAGER_C$ to function as a coincidence detector are largely controlled by the nanobody affinity (Extended Data Fig. 10f,g). Our observations suggest that $PAGER_C$ operates by a similar steric occlusion mechanism to $PAGER_{TF}$ and highlight the importance of balancing strong antagonism with facile displacement by antigens.

Customized cell behaviours driven by $PAGER_C$

We explored the ability of $PAGER_C$ to produce customized cellular responses to antigens specified by the nanobody component of $PAGER$. In neurons, G_q and G_i signalling can produce activation or silencing of neuronal activity, respectively, and this has led to the widespread use of G_q - and G_i -coupled DREADDs for drug-dependent modulation of neuronal function¹². $PAGER_C$ applications go beyond DREADDs by conferring antigen dependence, enabling activation or inhibition of neuronal activity only when both drug and soluble or cell-surface antigen are present.

To test $PAGER_C$ in this context, we transduced cultured rat cortical neurons with anti-mCherry $PAGER_{G_q}$ and fluorescent DAG-binding probe. Stimulation of neurons with recombinant mCherry and CNO, but not CNO alone, produced DAG synthesis at the plasma membrane (Extended Data Fig. 11a,b). We also plated mCherry-expressing HEK cells on top of cultured neurons expressing anti-mCherry $PAGER_{G_q}$ (Fig. 4a). When CNO was added, the DAG probe accumulated at HEK–neuron contact sites, consistent with local G_q activation and DAG lipid synthesis (Extended Data Fig. 11c).

Next, to test the ability of $PAGER_{G_i}$ to confer antigen-dependent neuronal inhibition, we transduced cultured neurons with anti-mCherry $PAGER_{G_i}$ and the calcium indicator GCaMP6s for real-time imaging of neuronal activity. Untreated neurons and CNO or DCZ-only treated neurons exhibited transient fluctuations in basal calcium (Fig. 4b, Extended Data Fig. 11d and Supplementary Video 1). However, addition of soluble mCherry along with CNO or DCZ strongly suppressed calcium activity within seconds, as did co-culturing with HEK cells that express cell-surface mCherry (Fig. 4c,d, Extended Data Fig. 11e,f and Supplementary Videos 2 and 3). These examples show that $PAGER_C$ has the potential to be used for spatially specific control of neuronal activity with genetically targetable antigens.

We then tested $PAGER_{G_i}$ in the more complex setting of intact mammalian brain tissue. Adult mice were injected with adeno-associated virus (AAV) encoding anti-mCherry $PAGER_{G_i}$ (LaM6- $PAGER_{G_i}$ -P2A-mEGFP) under a pan-neuronal synapsin promoter. Acute slices were prepared from the hippocampus and whole-cell patch clamp was used to record from CA1 neurons displaying GFP expression (Fig. 4e,f). Cell-intrinsic properties were evaluated before, during and after a 2-min bath application of 100 nM DCZ, either alone or paired with soluble mCherry to activate $PAGER$. Samples in the mCherry group were preincubated in 1 μ M mCherry for more than 30 min to ensure sufficient time for antigen penetration into brain slices.

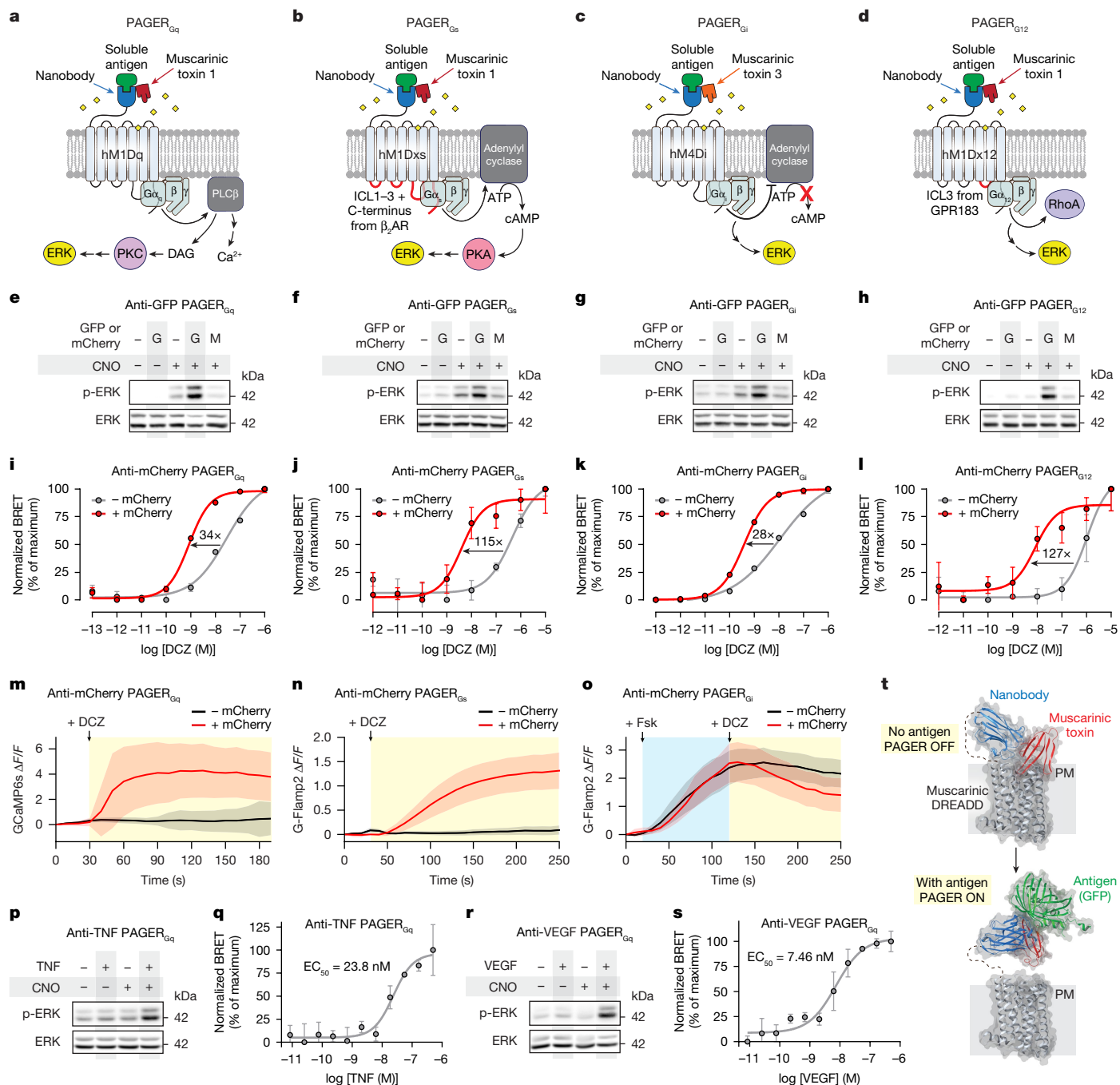


Fig. 3 | PAGER_{G} couples antigen recognition to activation of endogenous G-protein signalling. **a–d**, Schematics for PAGER_{Gq} (**a**), PAGER_{Gs} (**b**), PAGER_{Gi} (**c**) and $\text{PAGER}_{\text{G12}}$ (**d**), showing designs and downstream signalling induced by their activation. $\beta_2\text{AR}$, β_2 -adrenergic receptor. **e–h**, Western blots showing phosphorylation of ERK (p-ERK) in response to activation of PAGER_{Gq} (**e**), PAGER_{Gs} (**f**), PAGER_{Gi} (**g**) and $\text{PAGER}_{\text{G12}}$ (**h**). G and M indicate GFP and mCherry, respectively. HEK cells were stimulated with 100 nM CNO and 1 μM GFP for 5 min before analysis. $n = 3$ independent experiments. **i–l**, DCZ dose–response curves for PAGER_{Gq} -mediated (**i**), PAGER_{Gs} -mediated (**j**), PAGER_{Gi} -mediated (**k**) and $\text{PAGER}_{\text{G12}}$ -mediated (**l**) G-protein activation using TRUPATH BRET assay. HEK cells were stimulated with 1 μM mCherry. $n = 4$ independent experiments, 3 replicates per condition. Data are mean \pm s.d. **m–o**, Representative kinetic measurements of second messenger levels in HEK cells expressing anti-mCherry PAGER_{Gq} (**m**), PAGER_{Gs} (**n**) or PAGER_{Gi} (**o**). The calcium indicator GCaMP6s (for PAGER_{Gq}) or the cAMP indicator G-Flamp2 (for PAGER_{Gs} and PAGER_{Gi}) were

monitored by microscopy during the addition of 3 nM DCZ in the presence or absence of 1 μM mCherry. For PAGER_{Gi} , 2 μM forskolin (Fsk) was first added to increase cAMP levels prior to DCZ addition. $n = 50$ cells from 3 independent experiments. Data are mean \pm s.d. For kinetic measurements across a range of DCZ concentrations, see Extended Data Fig. 9. **p–s**, PAGER_{Gq} can be programmed to respond to different antigens. **p, r**, Western blots showing phosphorylation of ERK after 5-min stimulation with 100 nM CNO and 100 nM antigen for anti-TNF (**p**) and anti-VEGF (**r**) PAGER_{Gq} . $n = 3$ independent experiments. **q, s**, Antigen dose–response curves for anti-TNF (**q**) and anti-VEGF (**s**) PAGER_{Gq} -mediated G $_q$ protein activation using TRUPATH BRET assay. $n = 2$ independent experiments, 3 replicates per condition. Data are mean \pm s.d. **t**, AlphaFold2-predicted structure of PAGER_{Gq} showing auto-inhibition by muscarinic toxin (MT1, red) and release of auto-inhibition upon nanobody (blue) binding to antigen (GFP, green).

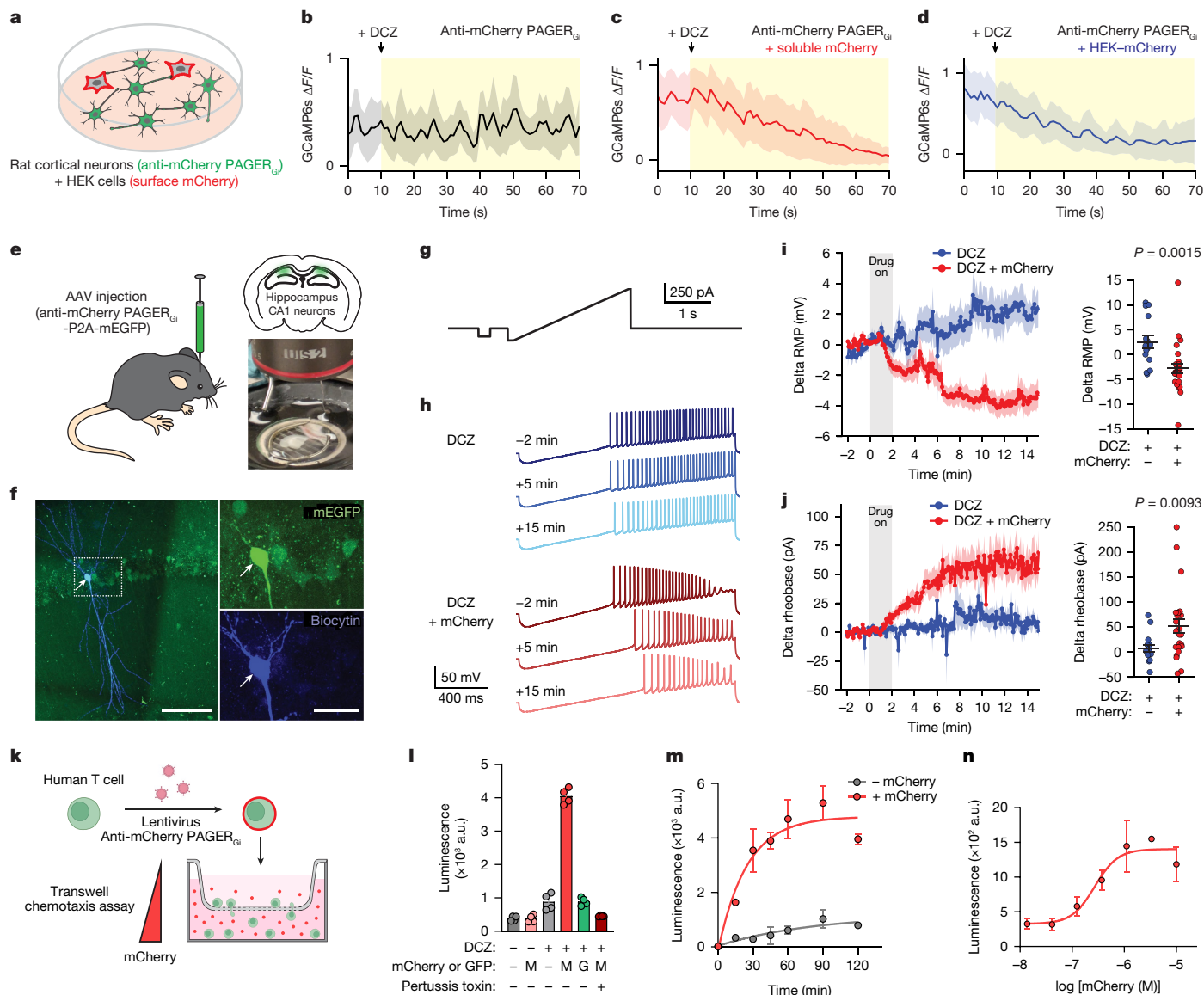


Fig. 4 | PAGER_G controls diverse cell behaviours in acute brain slices and primary T cells. **a**, Schematic of co-culture experiment for PAGER_G control of neuronal activity. **b–d**, Calcium traces in rat cortical neurons co-expressing anti-mCherry PAGER_G and GCaMP6s with or without soluble (1 μM) or surface mCherry. DCZ was added at $t = 10$ s to a final concentration of 2 nM. Data are mean \pm s.d. for $n = 50$ cells from 3 independent experiments. **e**, Schematic for PAGER_G-mediated neuronal inhibition in acute brain slices. **f**, Maximum intensity projection showing mEGFP labelling in PAGER_G-expressing neurons in CA1 (representative of $n = 14$ assessed cells). Biocytin labelling shows a recorded neuron (arrow). Scale bar: left, 100 μm; right, 30 μm. **g**, Current clamp protocol for monitoring intrinsic electrical property dynamics of PAGER_G-expressing neurons. **h**, Representative traces of evoked action potential alterations following DCZ (100 nM) with or without mCherry (1 μM) application. Neurons displayed greater intrinsic property shifts associated with reduced excitability when presented with DCZ plus mCherry rather than DCZ alone. **i, j**, Changes in

RMP (**i**) and rheobase currents required to evoke action potentials (**j**), upon 2-min DCZ addition. $n = 15$ cells, 7 mice (DCZ); $n = 26$ cells, 6 mice (DCZ plus mCherry). Data are mean \pm s.e.m. Mixed linear model regression analysis; $Z = 3.17, P = 0.0015$ (**i**); $Z = 2.60, P = 0.0093$ (**j**). **k**, Schematic for PAGER_G-mediated chemotaxis in Boyden chamber. T cells expressing anti-mCherry PAGER_G in the top chamber migrate through a porous membrane towards soluble mCherry in the bottom chamber. **l**, Bar graph representing the number of T cells in the bottom chamber after 2 h exposure to 10 μM mCherry in the bottom chamber. $n = 4$ independent experiments from 2 independent T cell donors, 4 replicates per condition. Data are mean \pm s.d. **m**, Time-course measurement of anti-mCherry PAGER_G T cell migration. $n = 2$ independent experiments, 4 replicates per condition. Data are mean \pm s.d. **n**, mCherry dose-response of anti-mCherry PAGER_G T cell migration. $n = 1$ independent experiment, 4 replicates. Data are mean \pm s.d.

We used a stepwise current injection followed by a continuous ramp protocol to monitor resting membrane potential (RMP), input resistance and rheobase values throughout each recording^{39,40} (Fig. 4g,h). Neurons displayed a greater hyperpolarizing shift in RMP when presented with DCZ plus mCherry than with DCZ alone (Fig. 4i). Similarly, the rheobase current needed to evoke action potentials increased in DCZ plus mCherry neurons, compared with DCZ-only samples (Fig. 4j). We also observed a similar time course trend for decreasing input resistance in DCZ plus mCherry neurons, consistent with hM4Di-mediated

inhibition⁴¹, and no correlation between PAGER expression and baseline electrophysiology responses in neurons (Extended Data Fig. 12). Our results are consistent with PAGER_G providing antigen-dependent control of neuronal activity when expressed in the mouse brain.

We then explored the utility of PAGER_G for controlling the behaviour of T cells. The migration of T cells into solid tumours is a limiting factor for overall survival in patients with cancer, and therefore strategies to modulate the homing of T cells are of therapeutic interest⁴². Chemokine receptors are natural G_i-coupled GPCRs that stimulate the directed migration

of many cell types along a chemical gradient⁴³. We hypothesized that PAGER_{Gi} could potentially recapitulate the G_i signalling downstream of chemokine receptors and thereby drive T cell chemotaxis toward an arbitrary antigen⁴⁴. To test this, we transduced human primary T cells with anti-mCherry PAGER_{Gi} and used a transwell chemotaxis assay to assess migration along an mCherry gradient (Fig. 4l). We observed that T cells expressing anti-mCherry PAGER_{Gi} (Extended Data Fig. 12h) migrate towards mCherry in the presence of DCZ, but not towards a non-cognate antigen (GFP) (Fig. 4m). Inhibition of G_i activation using pertussis toxin blocked PAGER-mediated migration, suggesting that PAGER mediates chemotaxis through a similar pathway to native chemokine receptors. In a time-course experiment, we could detect PAGER-mediated migration within minutes of antigen exposure (Fig. 4n), and as little as 100 nM mCherry was needed to stimulate migration (Fig. 4o). Collectively, our data suggest that PAGER_c can be used to reprogram complex cellular behaviours in response to soluble or cell-attached antigens of interest.

Real-time fluorescent sensors based on PAGER

As a third readout, we explored the use of PAGER for real-time fluorescence detection of antigen binding to cells. GPCR activation-based sensors (GRABs) are a class of sensors that are widely used in neuroscience for real-time fluorescence detection of neurotransmitters, neuromodulators and neuropeptides^{45,46}. GRABs are designed from GPCRs and install a conformation-sensitive circularly permuted fluorescent protein between transmembrane segments 5 and 6 to respond to binding of the receptors to their cognate ligands. Many antigens of interest, however, do not have natural GPCRs that can be exploited for development of GRAB-type sensors. In these cases, we explored whether PAGER fused to conformation-sensitive circularly permuted GFP (cpEGFP) could be used for real-time detection of diverse antigens (PAGER_{FL}).

First, we attempted to develop a GRAB-type sensor from M4 DREADD (Extended Data Fig. 13a,b), from which PAGER_{Gi} was made. Starting from wild-type human M4, we inserted cpEGFP between transmembrane segments 5 and 6, screened many linkers on either side of cpEGFP, optimized the cpEGFP sequence, and obtained an acetylcholine (ACh) sensor, hM4-1.0, with good membrane trafficking, a maximal response of around twofold, and an apparent affinity of approximately 225 nM (Extended Data Fig. 13c–e). We then introduced the DREADD binding pocket mutations into hM4-1.0 (Extended Data Fig. 13f), producing DCZ1.0, which resulted in 1.7-fold fluorescence turn-on in response to the DREADD ligand DCZ and other designed drugs (Extended Data Fig. 13g–j). We confirmed that this sensor does not couple with downstream G_i protein, unlike hM4Di (Extended Data Fig. 13k), thus minimizing its potential to perturb native biology.

From DCZ1.0, we produced our first PAGER_{FL} that was responsive to mCherry antigen (anti-mCherry PAGER_{FL}) by appending the mCherry nanobody LaM6 fused to the inhibitory toxin MT3 (Fig. 5a,b). Fluorescence measurements showed 300-fold sensitization to DCZ in the presence of mCherry but not non-cognate antigen (BFP) (Fig. 5c–e). Anti-BFP PAGER_{FL}, generated by replacing LaM6 with the GFP- and BFP-binding LaG2 nanobody, showed 130-fold sensitization to DCZ in the presence of BFP but not mCherry (Fig. 5f–h). We then performed time-lapse imaging in HEK cells with sequential addition of DCZ and antigen (Fig. 5i–l). Whereas binding of mCherry to anti-mCherry PAGER_{FL} was rapid (time constant (t_{50}) = 24 s), the green fluorescence response of PAGER_{FL} was slower, with a t_{50} of 3.1 min. This lag time may reflect the mechanism of PAGER_{FL}, in which the EGFP-enhancing conformational change occurs only after toxin unbinding, mCherry binding and DCZ-mediated activation. Nonetheless, PAGER_{FL} gives much faster readout than PAGER_{TF} (translational readout occurs 4–24 h after antigen exposure; Extended Data Fig. 3e) and should enable applications that are not accessible to PAGER_{TF}.

To test the modularity of PAGER_{FL}, we replaced the GFP-binding nanobody with nanobodies against TNF (ozoralizumab) or VEGF (Nb35).

Anti-TNF PAGER_{FL} localized well to the plasma membrane of HEK 293T cells, and the application of 1 μ M TNF elicited fluorescence increase in the presence of DCZ (Fig. 5m,n). The response magnitude ($\Delta F/F_0$) and kinetics of anti-TNF PAGER_{FL} and anti-VEGF PAGER_{FL} were similar to those of anti-mCherry PAGER_{FL} (Fig. 5o,p and Extended Data Fig. 13l,m). Collectively, our results show that PAGER can be successfully merged with the GRAB sensor scaffold to enable real-time detection of antigens.

Discussion

PAGER is a versatile platform for the detection of diverse extracellular signals and conversion into a range of user-specified intracellular responses. The high modularity of PAGER, its ability to respond to both surface and soluble antigens, the built-in drug gating, and its ability to drive antigen-dependent transgene expression, G-protein activation or real-time fluorescence distinguish this platform from other technologies and suggest broad applicability in cell biology and neuroscience.

Early strategies to develop synthetic receptors focused on mutation of natural receptors via site-directed mutagenesis^{8,9} or directed evolution^{10,11} to alter ligand specificity. This approach is generally time-, labour- and resource-intensive and needs to be repeated for every new synthetic receptor. An alternative approach alters ligand specificity by replacing the sensing domains of native receptors with other ligand-binding domains such as single-chain antibody variable fragments (scFvs) or nanobodies. This more modular approach has produced chimeric antigen receptors³, synthetic Notch receptor⁴ (syn-Notch), synthetic intramembrane proteolysis receptors⁵ (SNIPRs), modular extracellular sensor architecture (MESA) receptors⁶ and generalized extracellular molecule sensor (GEMS) receptors⁷.

Despite their considerable contributions to advancing mammalian cell engineering, particularly with regards to therapeutics, these technologies still have important limitations. One prevailing constraint is the general lack of ability to respond to soluble antigens. A few examples have addressed this by using two non-overlapping binders against a single antigen to drive receptor dimerization^{6,7}. However, suitable pairs of antigen recognition domains are rarely available, limiting the generalizability of this approach. Other platforms⁴⁷ have been shown to work with dimeric antigens that drive receptor clustering and endocytosis; since many antigens of interest are not dimeric, however, the scope of such methods is limited.

By contrast, PAGER requires a single antigen-binding domain and converts it into a synthetic receptor for detection of tethered or soluble antigens in a single cloning step. PAGER works on a multitude of antigen types, including monomeric and multimeric antigens. PAGER is also differentiated from other technologies by its built-in drug control, which provides temporal specificity and increases signal-to-background ratio. Moreover, PAGER offers a diverse array of outputs, including transgene expression, fluorescence and control of endogenous G-protein pathways.

In the field of GPCR engineering, many powerful technologies have been developed to convert GPCR activation into a range of intracellular readouts, including BRET and Förster resonance energy transfer signals³⁰, fluorescence intensity changes^{45,48}, RNA editing⁴⁹ and gene expression driven by transcription factors^{14,15,50}, CRISPR–Cas9⁵¹ or response elements⁵². By providing new programmability on the input side of GPCRs—where much less progress has been made than on the output side—PAGER not only provides a new technology but can be merged with existing GPCR technologies to make them more useful. We demonstrate this here by creating PAGER_{TF} from SPARK components, and PAGER_{FL} from GRAB components, but many more fusions of PAGER with existing technologies are possible.

PAGER does have important limitations, which are explained in detail in Supplementary Information. We have also provided ‘General guidelines for designing and validating PAGERs’ in Methods, which provides detailed step-by-step instructions on how to design, validate, and use novel PAGERs.

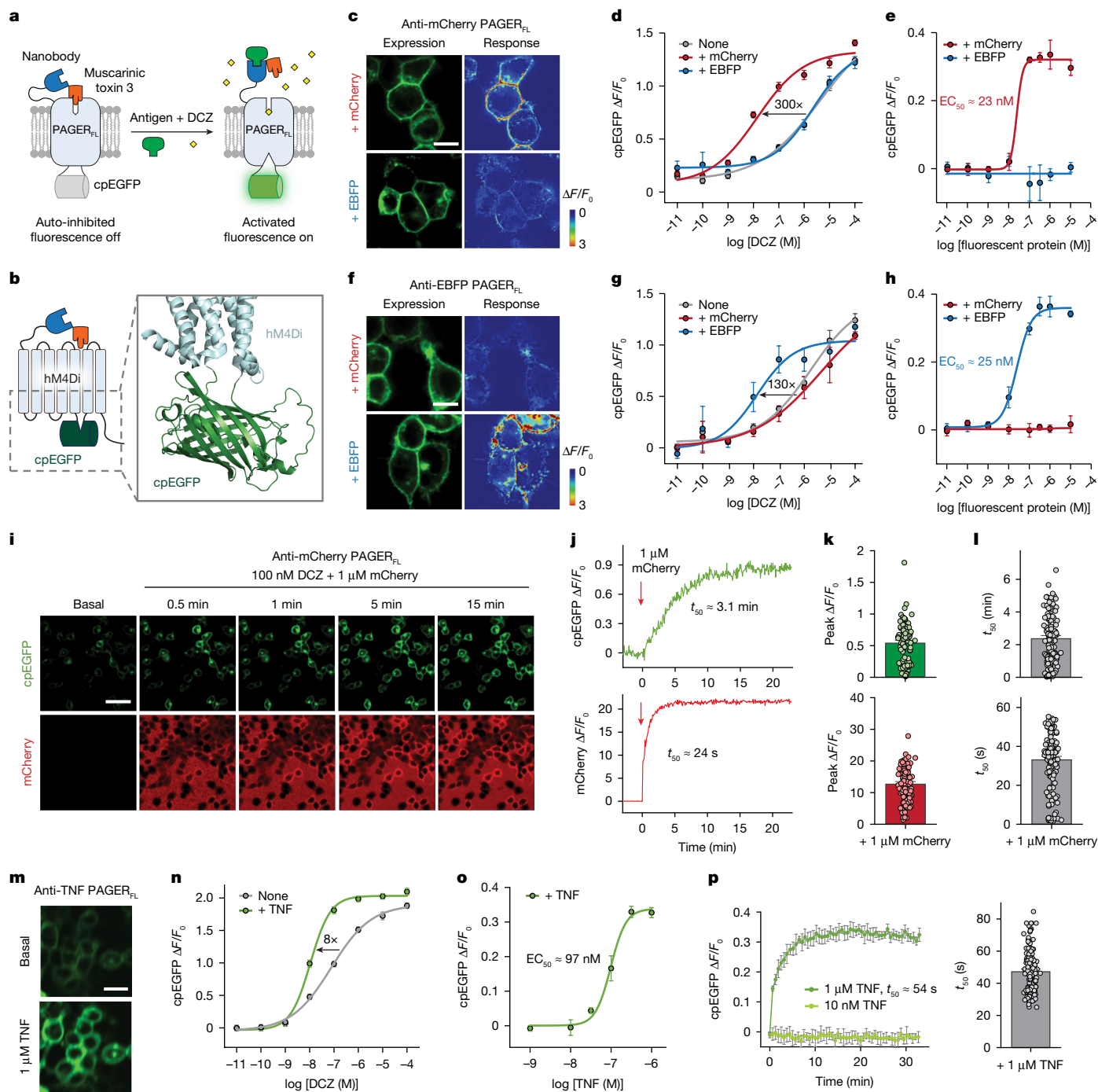


Fig. 5 | PAGER_{FL} for real-time fluorescence detection of extracellular antigens. **a**, Schematic of PAGER_{FL}, based on GRABs^{1,2}. PAGER_{FL} activation results in GPCR conformational changes, causing increased fluorescence of an inserted cpEGFP. **b**, Schematic and model structure of cpEGFP insertion between helices 5 and 6 in PAGER_{FL}. **c**, Representative images of expression and response of anti-mCherry PAGER_{FL} after 30 min treatment with 100 nM DCZ and 1 μM mCherry or EBFP (control). Scale bar, 10 μm. **d**, DCZ dose-response curves for anti-mCherry PAGER_{FL} ± 1 μM mCherry or EBFP. $n = 300$ cells from 3 independent experiments. Data are mean ± s.e.m. **e**, Antigen dose-response curves of anti-mCherry PAGER_{FL} with mCherry or EBFP and 100 nM DCZ. $n = 300$ cells from 3 independent experiments. Data are mean ± s.e.m. **f-h**, As c-e, but with anti-EBFP PAGER_{FL}. Scale bar, 10 μm. Data are mean ± s.e.m. **i**, Representative images of anti-mCherry PAGER_{FL} at various timepoints after 1 μM mCherry addition. $n = 3$ independent experiments. Scale bar, 50 μm. **j**, Time traces of

mCherry and cpEGFP fluorescence from **i**, **k**, Summary data for peak response of mCherry and cpEGFP fluorescence in anti-mCherry PAGER_{FL}. $n = 96$ cells from 3 independent experiments. Data are mean ± s.e.m. **l**, Summary data showing the t_{50} of mCherry and cpEGFP fluorescence in anti-mCherry PAGER_{FL}. $n = 144$ cells from 4 independent experiments. Data are mean ± s.e.m. **m**, Representative images of anti-TNF PAGER_{FL} before versus after 1 μM TNF addition in the presence of 100 nM DCZ. $n = 3$ independent experiments. Scale bar, 20 μm. **n**, DCZ dose-response curves for anti-TNF PAGER_{FL} with or without 300 nM TNF. $n = 300$ cells from 3 independent experiments. Data are mean ± s.e.m. **o**, TNF dose-response curve for anti-TNF PAGER_{FL} with 100 nM DCZ. $n = 300$ cells from 3 independent experiments. Data are mean ± s.e.m. **p**, Time traces (left) and summary data (right) of cpEGFP fluorescence response for anti-TNF PAGER_{FL}. $n = 137$ cells from 3 independent experiments. Data are mean ± s.e.m.

In future work, the PAGER platform could be improved and extended in a number of ways. Instead of requiring three separate transgenes, the design of PAGER_{TF} could be simplified to require only two, similar to how we simplified our calcium integrator FLARE⁵³ to produce single-chain FLARE⁵⁴ (scFLARE). For *in vivo* applications, it would be beneficial to remove the requirement for light or furimazine¹⁵, which are currently needed to uncage the LOV domain of PAGER_{TF}. To improve the orthogonality of PAGER_{TF}, we could mutate its intracellular loops to abolish recognition of G_i, drawing inspiration from a DREADD that recruits arrestin without coupling to any of the G proteins⁵⁵. Finally, we note that PAGER's antigen-gated, auto-inhibited design could be extended to other classes of proteins beyond GPCRs—for example, to produce antigen-gated enzymes or ion channels.

Online content

Any methods, additional references, Nature Portfolio reporting summaries, source data, extended data, supplementary information, acknowledgements, peer review information; details of author contributions and competing interests; and statements of data and code availability are available at <https://doi.org/10.1038/s41586-024-08282-3>.

- Mitra, A. et al. From bench to bedside: the history and progress of CAR T cell therapy. *Front. Immunol.* **14**, 1188049 (2023).
- Larson, R. C. & Maus, M. V. Recent advances and discoveries in the mechanisms and functions of CAR T cells. *Nat. Rev. Cancer* **21**, 145–161 (2021).
- Labanieh, L. & Mackall, C. L. CAR immune cells: design principles, resistance and the next generation. *Nature* **614**, 635–648 (2023).
- Morsut, L. et al. Engineering customized cell sensing and response behaviors using synthetic Notch receptors. *Cell* **164**, 780–791 (2016).
- Zhu, I. et al. Modular design of synthetic receptors for programmed gene regulation in cell therapies. *Cell* **185**, 1431–1443.e16 (2022).
- Daringer, N. M., Dudek, R. M., Schwarz, K. A. & Leonard, J. N. Modular extracellular sensor architecture for engineering mammalian cell-based devices. *ACS Synth. Biol.* **3**, 892–902 (2014).
- Scheller, L., Strittmatter, T., Fuchs, D., Bojar, D. & Fussenegger, M. Generalized extracellular molecule sensor platform for programming cellular behavior. *Nat. Chem. Biol.* **14**, 723–729 (2018).
- Jacobson, K. A., Gao, Z.-G. & Liang, B. T. Neoeptors: reengineering GPCRs to recognize tailored ligands. *Trends Pharmacol. Sci.* **28**, 111–116 (2007).
- Vardy, E. et al. A new DREADD facilitates the multiplexed chemogenetic interrogation of behavior. *Neuron* **86**, 936–946 (2015).
- Di Roberto, R. B., Chang, B. & Peisajovich, S. G. The directed evolution of ligand specificity in a GPCR and the unequal contributions of efficacy and affinity. *Sci. Rep.* **7**, 16012 (2017).
- Armbruster, B. N., Li, X., Pausch, M. H., Herlitze, S. & Roth, B. L. Evolving the lock to fit the key to create a family of G protein-coupled receptors potently activated by an inert ligand. *Proc. Natl Acad. Sci. USA* **104**, 5163–5168 (2007).
- Roth, B. L. DREADDs for neuroscientists. *Neuron* **89**, 683–694 (2016).
- Wang, Y. et al. Structures of the entire human opioid receptor family. *Cell* **186**, 413–427.e17 (2023).
- Kim, M. W. et al. Time-gated detection of protein–protein interactions with transcriptional readout. *eLife* **6**, e30233 (2017).
- Kim, C. K., Cho, K. F., Kim, M. W. & Ting, A. Y. Luciferase-LOV BRET enables versatile and specific transcriptional readout of cellular protein–protein interactions. *eLife* **8**, e43826 (2019).
- Carroll, F. I. & Carlezon, W. A. Development of κ opioid receptor antagonists. *J. Med. Chem.* **56**, 2178–2195 (2013).
- Fridy, P. C. et al. A robust pipeline for rapid production of versatile nanobody repertoires. *Nat. Methods* **11**, 1253–1260 (2014).
- Schoof, M. et al. An ultrapotent synthetic nanobody neutralizes SARS-CoV-2 by stabilizing inactive Spike. *Science* **370**, 1473–1479 (2020).
- Wheeler, K. C. et al. VEGF may contribute to macrophage recruitment and M2 polarization in the decidua. *PLoS ONE* **13**, e0191040 (2018).
- Sierra-Filardi, E. et al. CCL2 shapes macrophage polarization by GM-CSF and M-CSF: identification of CCL2/CCR2-dependent gene expression profile. *J. Immunol.* **192**, 3858–3867 (2014).
- Gianchechi, E., Delfino, D. V. & Fierabracci, A. Recent insights into the role of the PD-1/PD-L1 pathway in immunological tolerance and autoimmunity. *Autoimmun. Rev.* **12**, 1091–1100 (2013).
- Goebeler, M.-E. & Bargou, R. C. T cell-engaging therapies — BiTEs and beyond. *Nat. Rev. Clin. Oncol.* **17**, 418–434 (2020).
- Li, M., Knight, D. A., Snyder, L. A., Smyth, M. J. & Stewart, T. J. A role for CCL2 in both tumor progression and immunosurveillance. *Oncotarget* **2**, e25474 (2013).
- Blank, C., Gajewski, T. F. & Mackensen, A. Interaction of PD-L1 on tumor cells with PD-1 on tumor-specific T cells as a mechanism of immune evasion: implications for tumor immunotherapy. *Cancer Immunol. Immunother.* **54**, 307–314 (2005).
- Schulz, R., Korkut-Demirbaş, M., Venturino, A., Colombo, G. & Siegert, S. Chimeric GPCRs mimic distinct signaling pathways and modulate microglia responses. *Nat. Commun.* **13**, 4728 (2022).
- Inoue, A. et al. Illuminating G-protein-coupling selectivity of GPCRs. *Cell* **177**, 1933–1947.e25 (2019).
- Nagai, Y. et al. Deschloroclozapine, a potent and selective chemogenetic actuator enables rapid neuronal and behavioral modulations in mice and monkeys. *Nat. Neurosci.* **23**, 1157–1167 (2020).
- Servent, D. & Fruchart-Gaillard, C. Muscarinic toxins: tools for the study of the pharmacological and functional properties of muscarinic receptors. *J. Neurochem.* **109**, 1193–1202 (2009).
- Maeda, S. et al. Structure and selectivity engineering of the M1 muscarinic receptor toxin complex. *Science* **369**, 161–167 (2020).
- DiBerto, J. F., Olsen, R. H. J. & Roth, B. L. In *Bioluminescence: Methods and Protocols*, vol. 2 (ed. Kim, S.-B.) 185–195 (Springer, 2022); https://doi.org/10.1007/978-1-0716-2473-9_13.
- Oancea, E., Teruel, M. N., Quest, A. F. G. & Meyer, T. Green fluorescent protein (GFP)-tagged cysteine-rich domains from protein kinase C as fluorescent indicators for diacylglycerol signaling in living cells. *J. Cell Biol.* **140**, 485–498 (1998).
- Chen, T.-W. et al. Ultra-sensitive fluorescent proteins for imaging neuronal activity. *Nature* **499**, 295–300 (2013).
- Liu, W., Liu, C., Ren, P.-G., Chu, J. & Wang, L. An improved genetically encoded fluorescent cAMP indicator for sensitive cAMP imaging and fast drug screening. *Front. Pharmacol.* **13**, 902290 (2022).
- Ishiwatari-Ogata, C. et al. Ozoralizumab, a humanized anti-TNF α nanobody compound, exhibits efficacy not only at the onset of arthritis in a human TNF transgenic mouse but also during secondary failure of administration of an Anti-TNF α IgG. *Front. Immunol.* **13**, 853008 (2022).
- Veritti, D., Sarao, V., Gorni, G. & Lanzetta, P. Anti-VEGF drugs dynamics: relevance for clinical practice. *Pharmaceutics* **14**, 265 (2022).
- Parameswaran, N. & Patial, S. Tumor necrosis factor- α signaling in macrophages. *Crit. Rev. Eukaryot. Gene Expr.* **20**, 87–103 (2010).
- Duffy, A. M., Bouchier-Hayes, D. J. & Harme, J. H. In *Madame Curie Bioscience Database* (Landes Bioscience, 2013).
- Raimondo, F. et al. Elevated vascular endothelial growth factor (VEGF) serum levels in idiopathic myelofibrosis. *Leukemia* **15**, 976–980 (2001).
- Zhu, H. et al. Chemogenetic inactivation of ventral hippocampal glutamatergic neurons disrupts consolidation of contextual fear memory. *Neuropsychopharmacol.* **39**, 1880–1892 (2014).
- Nguyen, Q.-A. et al. Acetylcholine receptor based chemogenetics engineered for neuronal inhibition and seizure control assessed in mice. *Nat. Commun.* **15**, 601 (2024).
- Shan, Q., Fang, Q. & Tian, Y. Evidence that GIRK channels mediate the DREADD-hM4Di receptor activation-induced reduction in membrane excitability of striatal medium spiny neurons. *ACS Chem. Neurosci.* **13**, 2084–2091 (2022).
- Melero, I., Rouzaut, A., Motz, G. T. & Coukos, G. T-Cell and NK-Cell Infiltration into Solid Tumors: A Key Limiting Factor for Efficacious Cancer Immunotherapy. *Cancer Discov.* **4**, 522–526 (2014).
- Neptune, E. R. & Bourne, H. R. Receptors induce chemotaxis by releasing the $\beta\gamma$ subunit of G_i, not by activating G_q or G_s. *Proc. Natl Acad. Sci.* **94**, 14489–14494 (1997).
- Park, J. S. et al. Synthetic control of mammalian-cell motility by engineering chemotaxis to an orthogonal bioinert chemical signal. *Proc. Natl Acad. Sci.* **111**, 5896–5901 (2014).
- Wang, H. et al. A tool kit of highly selective and sensitive genetically encoded neuropeptide sensors. *Science* **382**, eabq8173 (2023).
- Jing, M. et al. An optimized acetylcholine sensor for monitoring *in vivo* cholinergic activity. *Nat. Methods* **17**, 1139–1146 (2020).
- Piraner, D. I. et al. Engineered receptors for soluble cellular communication and disease sensing. *Nature* <https://doi.org/10.1038/s41586-024-08366-0> (2024).
- Huppertz, M.-C. et al. Recording physiological history of cells with chemical labeling. *Science* **383**, 890–897 (2024).
- Zhang, X. et al. Post-transcriptional modular synthetic receptors. Preprint at *bioRxiv* <https://doi.org/10.1101/2024.05.03.592453> (2024).
- Barnea, G. et al. The genetic design of signaling cascades to record receptor activation. *Proc. Natl Acad. Sci. USA* **105**, 64–69 (2008).
- Kipniss, N. H. et al. Engineering cell sensing and responses using a GPCR-coupled CRISPR–Cas system. *Nat. Commun.* **8**, 2212 (2017).
- Cheng, Z. et al. Luciferase reporter assay system for deciphering GPCR pathways. *Curr. Chem. Genomics* **4**, 84–91 (2010).
- Wang, W. et al. A light- and calcium-gated transcription factor for imaging and manipulating activated neurons. *Nat. Biotechnol.* **35**, 864–871 (2017).
- Sanchez, M. I., Nguyen, Q.-A., Wang, W., Soltesz, I. & Ting, A. Y. Transcriptional readout of neuronal activity via an engineered Ca²⁺-activated protease. *Proc. Natl Acad. Sci. USA* **117**, 33186–33196 (2020).
- Nakajima, K. & Wess, J. Design and functional characterization of a novel, arrestin-biased designer G protein-coupled receptor. *Mol. Pharmacol.* **82**, 575–582 (2012).

Publisher's note Springer Nature remains neutral with regard to jurisdictional claims in published maps and institutional affiliations.



Open Access This article is licensed under a Creative Commons Attribution-NonCommercial-NoDerivatives 4.0 International License, which permits any non-commercial use, sharing, distribution and reproduction in any medium or format, as long as you give appropriate credit to the original author(s) and the source, provide a link to the Creative Commons licence, and indicate if you modified the licensed material. You do not have permission under this licence to share adapted material derived from this article or parts of it. The images or other third party material in this article are included in the article's Creative Commons licence, unless indicated otherwise in a credit line to the material. If material is not included in the article's Creative Commons licence and your intended use is not permitted by statutory regulation or exceeds the permitted use, you will need to obtain permission directly from the copyright holder. To view a copy of this licence, visit <http://creativecommons.org/licenses/by-nc-nd/4.0/>.

© The Author(s) 2024

Methods

Plasmid constructs and cloning

Constructs used for transient expression in HEK293T cells were cloned into the pAAV viral vector. For stable expression, the constructs were cloned into the pCDH viral vector. For all constructs, standard cloning procedures were used. PCR fragments were amplified using Q5 polymerase (NEB). Vectors were digested with NEB restriction enzymes and ligated to gel-purified PCR products using T4 ligation, Gibson, NEB HiFi, or Golden Gate assembly. Ligated plasmids were introduced into competent XL1-Blue, NEB5-alpha, or NEB Stable bacteria via heat shock transformation.

Cell lines

HEK293T and RAW 264.7 cells were obtained from ATCC (tested negative for mycoplasma) and cultured as monolayers in complete growth medium: Dulbecco's Modified Eagle Medium (DMEM, Corning) containing 4.5 g l⁻¹ glucose and supplemented with 10% Fetal Bovine Serum (FBS, VWR), 1% (v/v) GlutaMAX (Gibco), and 1% (v/v) Penicillin-Streptomycin (Corning, 5,000 units ml⁻¹ of penicillin and 5,000 µg ml⁻¹ streptomycin). Nalm6 B-ALL cells stably expressing GFP and firefly luciferase (Nalm6-GL) cells were provided by Crystal Mackall and cultured between 0.25–1.5 × 10⁶ cells per ml in complete growth medium: RPMI-1640 Medium (Corning) supplemented with 10% Fetal Bovine Serum (FBS, VWR), 1% (v/v) GlutaMAX (Gibco), and 1% (v/v) Penicillin-Streptomycin (Corning, 5,000 units ml⁻¹ of penicillin and 5,000 µg ml⁻¹ streptomycin). All cell lines were cultured at 37 °C under 5% CO₂. For experimental assays, HEK293T cells were grown in 6-well, 12-well, 24-well, or 96-well plates pretreated with 20 µg ml⁻¹ human fibronectin (Millipore) for at least 10 min at 37 °C.

Source of primary human T cells

Buffy coats from healthy donors were purchased from the Stanford Blood Center under an IRB-exempt-protocol. Primary human T cells were purified by negative selection using the RosetteSep Human T cell Enrichment kit (StemCell Technologies) and SepMate-50 tubes. T cells were cryopreserved at 4 × 10⁶ cells per ml in CryoStor CS10 cryopreservation medium (StemCell Technologies) until use. T cells were cultured in complete growth medium: RPMI-1640 Medium (Corning) supplemented with 10% Fetal Bovine Serum (FBS, VWR), 1% (v/v) GlutaMAX (Gibco), 40 units ml⁻¹ rhIL-2 (PeptoTech), and 1% (v/v) Penicillin-Streptomycin (Corning, 5,000 units ml⁻¹ of penicillin and 5,000 µg ml⁻¹ streptomycin).

Expression and purification of recombinant GFP and mCherry

Recombinant His-tagged GFP and mCherry were expressed in *E. coli* BL21(DE3). In brief, a 5 ml starter culture in 2× YT supplemented with antibiotic was grown overnight at 37 °C. The starter culture was diluted into 1 l of the same medium and grown at 37 °C to an OD₆₀₀ of ~0.8. and induced with 1 mM IPTG at 22 °C for 18 h. Cells were collected by centrifugation and lysed with Bacterial Protein Extraction Reagent (BPER, Thermo Scientific) supplemented with protease inhibitor cocktail per the manufacturer's instructions. Lysate was filtered using a 5-µm syringe filter and purified by FPLC on a Ni-NTA column. Eluted protein was dialysed overnight at 4 °C into 20 mM Tris pH 7.5, 150 mM NaCl. GFP storage buffer included 1 mM TCEP. Protein concentration was determined with spectrophotometry and diluted to 500 µM. Protein was aliquoted and frozen at -80 °C for long term storage.

HEK293T cell transient transfection

A 1 mg ml⁻¹ solution of PEI Max (Polysciences, 24765) was prepared for transient transfection as follows. Polyethylenimine (PEI, 500 mg) was added to 450 ml of Milli-Q H₂O in a 500 ml glass beaker while stirring with a stir bar. Concentrated HCL was added dropwise to the solution until the pH was less than 2.0. The PEI solution was stirred until PEI was

dissolved (~2–3 h). Concentrated NaOH was then added dropwise to the solution until the pH was 7.0. The volume of the solution was then adjusted to 500 ml, filter-sterilized through a 0.22-µm membrane, and frozen in aliquots at -20 °C. Working stocks were kept at 4 °C for no more than 1 month.

For transient transfection, HEK293T cells were grown in 6-well, 12-well, or 24-well plates pretreated with 20 µg ml⁻¹ human fibronectin (Millipore) for at least 10 min at 37 °C. Cells were grown to a confluency of ~70–90% prior to transfection. DNA transfection complexes were made by mixing DNA and 1 mg ml⁻¹ PEI solution in serum-free DMEM at a 1 µg DNA: 5 µl PEI (1 mg ml⁻¹): 100 µl serum-free DMEM. Complexes were allowed to form for 20 min at room temperature. After 20 min, complexes were diluted in complete DMEM up to the growth volume per well size (2.5 ml for 6-well, 1 ml for 12-well, and 500 µl for 24-well). The entire well volume of the HEK293T cells was replaced with the diluted complexes and allowed to transfect cells at 37 °C for 5–24 h. Complete transfection protocols including amounts of DNA and length of transfection are described for each experiment below.

Firefly luciferase reporter PAGER_{TF} experiments

HEK293T cells were plated in human fibronectin-coated 6-well dishes at a density of 750,000 cells per well and allowed to grow overnight (~18 h) at 37 °C until they reached ~70–90% confluency. After ~18 h, the cells were transfected with 350 ng of the indicated Antagonist-Nanobody-GPCR-eLOV-TEVcs-Gal4 (PAGER_{TF}) receptor plasmid, 100 ng of NanoLuc-β-arrestin2-TEVp plasmid, and 150 ng of UAS-Firefly Luciferase (FLuc) plasmid. Cells were transfected for 5 h at 37 °C. After 5 h of transfection, cells from each well were lifted and resuspended in 6 ml of complete DMEM to make an ~400,000 cells per ml single cell suspension, and 100 µl of cell suspension (~40,000 cells) was plated per well in a human fibronectin-coated white, clear bottom 96-well plate in triplicate. Plates were wrapped in aluminum foil to protect them from light and incubated at 37 °C overnight (~18 h). After ~18 h, cells should be stimulated.

Stimulation was performed in a dark room with a red light source (red light does not open the LOV domain). Stimulation solutions were optimized for each given antigen and PAGER receptor. Unless otherwise indicated, PAGERS were stimulated as follows: GFP (LaG17/LaG2/LaG16)-PAGERS were stimulated with 1 µM GFP, 1 µM SalB, and 1× furimazine; mCherry (LaM6)-PAGERS were stimulated with 1 µM mCherry, 1 µM SalB, and 1× furimazine; VEGF (Nb35)-PAGERS were stimulated with 500 nM VEGF, 500 nM SalB, and 1× furimazine; HGF (Nb1E2)-PAGERS were stimulated with 250 nM HGF, 250 nM SalB, and 1× furimazine; TNF (ozoralizumab)-PAGERS were stimulated with 500 nM TNF, 250 nM or 500 nM SalB, and 1× furimazine; IL-17 (Sonelokimab)-PAGER was stimulated with 500 nM IL-17, 100 nM SalB, and 1× furimazine; IL-23 (Nb22E11)-PAGER was stimulated with 250 nM IL-23, 500 nM SalB, and 1× furimazine; sL6R (Voberilizumab)-PAGER was stimulated with 500 nM sIL-6R, 500 nM SalB, and 1× furimazine; CCL2 (Nb8E10)-PAGER was stimulated with 1 µM CCL2, 500 nM SalB, and 1× furimazine; EGFR (NbEgB4)-PAGERS were stimulated with 500 nM EGFR ECD, 100 nM or 250 nM or 500 nM SalB, and 1× furimazine; HER2 (Nb2Rs15d)-PAGERS were stimulated with 500 nM HER2 ECD, 500 nM or 1 µM SalB, and 1× furimazine; CD38 (NbMU375)-PAGER was stimulated with 1 µM CD38 ECD, 500 nM SalB, and 1× furimazine; PD-L1 (KN035)-PAGER was stimulated with 1 SalBPD-L1 ECD, 500 nM SalB, and 1× furimazine; SARS-CoV-2 RBD (NbF2)-PAGER was stimulated with 200 nM SARS-CoV-2 spike protein, 500 nM or 1 µM SalB, and 1× furimazine; uPA (Nb4)-PAGER was stimulated with 500 nM uPA, 250 nM or 500 nM SalB, and 1× furimazine.

For stimulations, growth medium was removed from the 96-well plate by flicking off and dabbing excess on a paper towel. To initiate stimulation, 100 µl stimulation solution was added to each well for a total of 15 min. After 15 min, stimulation solution was removed by flicking off and dabbing excess on a paper towel, and 100 µl of

Article

complete DMEM was added back to each well. Plates were again wrapped in aluminum foil and placed in 37 °C incubator for 8 h. After 8 h post-stimulation, medium was removed from 96-well plate by flicking off and dabbing excess on paper towel. Wells were washed once with 125 µl DPBS, and then 50 µl of 1× Bright-Glo (2× diluted 1:1 in DPBS; Promega) was added to each well and incubated for 1 min. After 1 min, firefly luciferase luminescence was measured using a Tecan Infinite M1000 Pro plate reader using the following parameters: 1,000 ms acquisition time, green-1 filter (520–570 nm), 25 °C linear shaking for 10 s.

In experiments where TEVp was used to activate PAGER, 1 µM recombinant TEVp was added to PAGER-expressing cells for 90 min prior to stimulation. In some experiments where indicated, exogenous ambient room white light was used to uncage the LOV domain instead of furimazine-dependent NanoLuc BRET. In these experiments, furimazine was not included in the stimulation solutions; all else remained the same. In some experiments where indicated, SalB or antigen SalB n dose–response curves were analysed. In these experiments, the concentrations of SalB or antigen were included in the stimulation solutions at different concentrations as indicated; all else remained the same.

HEK293T co-culture for trans assays

For trans assays using co-plated HEK293T cells, cells were cultured in 6-well and 12-well plates as described above. Receiver cells in 12-well plates were transfected with 140 ng of the indicated pAAV-Antagonist-Nanobody-PAGER-eLOV-TEVcs-Gal4 receptor plasmid, 40 ng of pAAV-NanoLuc-βarrestin2-TEVp plasmid, and 60 ng of pAAV-UAS-Firefly Luciferase (FLuc) plasmid. Sender cells in 6-well plates were transfected with 2 µg of pAAV-GFP-PDGFR transmembrane domain (surface-expressed GFP). Cells were transfected for 5 h in a 37 °C incubator. After 5 h, cells were lifted with trypsin, washed with DPBS, and resuspended in 6.25 ml or 2.5 ml of complete DMEM per well for 6-well and 12-well plates, respectively. Sender and receiver cells were mixed at a 4:1 sender:receiver ratio and then 100 µl of cell mixtures were plated into 96-well white, clear-bottom microplates at a density of 40,000 cells per well. Plates were wrapped in aluminum foil and incubated for -18 h in a 37 °C incubator, then the stimulations and luciferase reporter assay were performed as described above.

HEK293T and macrophage differentiation co-culture assay

HEK293T cells were plated in human fibronectin-coated 6-well dishes at a density of 750,000 cells per well and allowed to grow overnight (-18 h) at 37 °C until they reached ~70–90% confluency. After -18 h, the cells were transfected with 350 ng of the indicated PAGER_{TF} receptor plasmid, 100 ng of NanoLuc-βarrestin2-TEVp plasmid, and 75 ng of UAS-mouse IFNγ plasmid. Cells were transfected for 5 h at 37 °C. After 5 h of transfection, cells from each well were lifted and resuspended to 1 × 10⁶ cells per ml in complete DMEM. 250 µl of cell suspension (~250,000 cells) were plated in the top chamber of fibronectin-coated 24-well Transwells (8-µm pore size). Plates were wrapped in aluminum foil to protect them from light and incubated at 37 °C overnight (-18 h). After -18 h, cells were stimulated in a dark room under red light with 100 µl of 500 nM Sal B, 1× furimazine, and antigen (2 µM mCherry, 500 nM VEGF, 500 nM CCL2, or 1 µM PD-L1) for 15 min. After 15 min, stimulations were removed and replaced with 200 µl complete DMEM. Immediately following stimulation, 400 µl of 2.5 × 10⁵ RAW 264.7 macrophage cells (~100,000 cells) were placed in the bottom chamber of the Transwell. A final concentration of 10 ng ml⁻¹ mouse IFNγ was added to the bottom chamber of the positive control well. Plates were then wrapped in aluminum foil to protect them from light and incubated at 37 °C for 48 h before being readout by imaging to assess morphological changes and qPCR with reverse transcription (RT–qPCR) to measure induction of the M1 macrophage markers CD86 and NOS2. Images of macrophages (at 20×) were taken using an Echo Rebel inverted microscope. Schematic summary of HEK293T

and macrophage differentiation co-culture assay was created, in part, using BioRender.

RT–qPCR for macrophage markers

At time of collection, the medium from each samples was aspirated, and cold D-PBS was immediately added to each well. The cells were then pelleted, and RNA was extracted using the RNeasy Mini Kit (Qiagen, 74104). To synthesize cDNA, 1 µg of total RNA (8 µl) from each group was combined with 2 µl of Superscript IV VILO Master Mix (Thermo Scientific, 11756050) and subjected to the following thermocycling protocol: 25 °C for 10 min, 50 °C for 10 min, and 85 °C for 5 min. After reverse transcription, the cDNA was diluted tenfold in nuclease-free water. qPCR was conducted in 384-well plates using the CFX Connect Real-Time System (Bio-Rad), with a total reaction volume of 10 µl per well. Each reaction consisted of 2.5 µl of diluted cDNA template, 2.5 µl of 1 µM forward and reverse primers, and 5 µl of 2× Maxima SYBR Green/ROX qPCR Master Mix (Thermo Scientific, K0221). The following primer sequences were used: UBC-FWD: GACCCTGACAGGCAAGACCATC; UBC-REV: CTGTGGTGAGGAAGGTACGTCTG; CD86-FWD: CTGTCAGTGATCGCCAACCTCAGTG; CD86-REV: CCTTGCTTAGACGTGCAGGTC; NOS2-FWD: CCTTGTGCTGTTCTACGCCAAC; NOS2-REV: CAGGGATTCTGGAACATTCTGTGC.

The thermal cycling protocol included an initial denaturation step at 95 °C for 3 min, followed by 40 cycles of 95 °C for 10 s and 60 °C for 30 s. A melt-curve analysis was performed from 65 °C to 95 °C, with 0.5 °C increments. Housekeeping gene Ubc was used as the reference gene for normalization. Data were analysed as follows: first, ΔCT was calculated as target CT – Ubc (housekeeping control) CT; second, ΔΔCT was calculated as target ΔCT – untreated (negative control) ΔCT; and finally, relative gene expression was calculated as 2^{-ΔΔCT} for each sample.

HEK293T, T cell and tumour killing co-culture assay

HEK293T cells were plated in human fibronectin-coated 6-well dishes at a density of 750,000 cells per well and allowed to grow overnight (-18 h) at 37 °C until they reached ~70–90% confluency. After -18 h, the cells were transfected with 350 ng of the indicated PAGER_{TF} receptor plasmid, 100 ng of NanoLuc-βarrestin2-TEVp plasmid, and 25 ng of UAS-CD3-CD19 BiTE plasmid. Cells were transfected for 5 h at 37 °C. After 5 h of transfection, cells from each well were lifted and resuspended in 6 ml of complete DMEM to make an ~400,000 cells per ml single cell suspension, and 100 µl of cell suspension (~40,000 cells) was plated per well in a human fibronectin-coated clear 96-well plate in triplicate. Plates were wrapped in aluminum foil to protect them from light and incubated at 37 °C overnight (-18 h). After -18 h, cells were stimulated in a dark room under red light with 50 µl of 250 nM Sal B, 1× furimazine, and antigen (2 µM GFP, 500 nM CCL2, or 1 µM PD-L1) for 15 min. After 15 min, stimulations were removed and replaced with 200 µl complete RPMI + 40 units ml⁻¹ human IL-2 containing 100,000 primary human T cells and 100,000 Nalm6-GL cells (1:1 effector:target). Plates were then wrapped in aluminum foil to protect them from light and incubated at 37 °C for 36 h. 30 µl aliquots were taken from each well every 10–12 h to measure tumour cells remaining over time. Stably expressed firefly luciferase in the Nalm6-GL cells was used to measure tumour cells remaining. To readout the amount of luciferase activity in each sample, 30 µl of 2× Bright-Glo (Promega) was added to the 30 µl cell aliquots from each samples and incubated for 1 min. After 1 min, firefly luciferase luminescence was measured using a Tecan Infinite M1000 Pro plate reader using the following parameters: 1,000 ms acquisition time, green-1 filter (520–570 nm), 25 °C linear shaking for 10 s. Schematic summary of HEK293T, T cell, and tumour killing co-culture assay was created, in part, using BioRender.

TRUPATH G-protein activation BRET assay

HEK293T cells were plated in human fibronectin-coated 6-well dishes at a density of 1,250,000 cells per well and allowed to adhere and grow for

2–4 h at 37 °C. After ~2–4 h, the cells were transfected 1:1:1 with 250 ng of the indicated G-protein PAGER receptor plasmid, 250 ng of the corresponding G α -RLuc8 TRUPATH plasmid (G α _S-RLuc8, G α _i-RLuc8 or G α ₁₂-RLuc8), 250 ng of G β 3 TRUPATH plasmid, and 250 ng Gy9-GFP2 TRUPATH plasmid. For G α _i1 TRUPATH with PAGER_{Gi}, a 1:1:1:1 ratio of components using 100 ng of each plasmid was used. Cells were incubated at 37 °C and transfection was allowed to proceed for ~20–24 h. After transfection, cells from each well were lifted and resuspended in 6 ml of complete DMEM to make an ~200,000 cells per ml single cell suspension, and 100 μ l of cell suspension (~20,000 cells) was plated per well in a human fibronectin-coated white, clear bottom 96-well plate in triplicate. Plates were incubated at 37 °C for ~20–24 h. For protease activation of G-protein-PAGERS, cells were treated with 1 μ M TEVp for 90 min followed by stimulation with various concentrations of CNO and 10 μ M CTZ400a (substrate for TRUPATH assay) for 5 min before reading out BRET. For antigen activation of PAGER_G's, cells were treated with 1 μ M mCherry for 15 min followed by stimulation with various concentrations of CNO and 10 μ M CTZ400a (for G α _i1 and G α _q TRUPATHs) or 10 μ M Prolume Purple (for G α _S and G α ₁₂ TRUPATHs) for 5 min before reading out BRET. BRET was readout using a Tecan Infinite M1000 Pro plate reader using the following parameters: filter 1 magenta (370 to 450 nm), 500 ms integration time; filter 2 green (510 to 540 nm), 500 ms integration time; 25 °C. Data are presented as NET BRET and displayed as scatter plots with variable slope (four parameter) non-linear regression lines.

Lentivirus generation

To generate lentivirus, HEK293T cells were cultured in T25 flasks and transfected at ~70% confluency with 2.5 μ g of the pCDH lentiviral transfer vector of interest and packaging plasmids psPAX2 (1.25 μ g) and pMD2.g (1.25 μ g) with 25 μ l PEI (1 mg ml⁻¹; Polysciences). Approximately 72 h post-transfection, the cell medium was collected and centrifuged for 5 min at 300g to remove cell debris. Medium containing lentivirus was used immediately for transduction or was aliquoted into 0.5 ml aliquots, flash-frozen in liquid nitrogen, and stored at -80 °C for later use. Frozen viral aliquots were thawed at 37 °C prior to infection.

HEK293T stable cell line generation

HEK293T cells were plated on six-well human fibronectin-coated plates. When cells reached ~70–90% confluency, cells were transduced with lentivirus for 1–3 days. The cells were then lifted and replated on a T25 flask, and stably expressing cells were selected for in complete DMEM containing 1 μ g ml⁻¹ puromycin for at least 1 week. Cells were split and expanded when they reached ~80–90% confluency. Cells were maintained under this puromycin selection until the time of experiments. Construct expression was confirmed by flow cytometry, immunofluorescence imaging, or functional characterization.

Quantification of p-ERK by western blotting

Antigen was added at indicated concentration to HEK 293T cells stably expressing PAGER_G. 3 min later, 300 nM of CNO in 500 μ l blank DMEM was added to a final concentration of 100 nM, and the cells were incubated for another 3 min. Cells were then lysed with RIPA lysis buffer supplemented with protease and phosphatase inhibitors (50 mM Tris-HCl, pH 7.4, 150 mM NaCl, 1% Triton X-100, 0.5% sodium deoxycholate, 0.1% SDS, 1 mM EDTA, 1 \times Halt Protease Inhibitor Cocktail from Thermo Scientific, 1 \times Phosphatase Inhibitor Cocktail from Cell Signaling Technology). After sonication and centrifugation, the lysate supernatants were mixed with 6 \times Laemmli sample buffer to prepare the sample for western blotting. The membrane was blotted with 1:1,000 dilutions of antibodies for phospho-p44/42 MAPK (phospho-Erk1/2; Cell Signaling Technology 9101), p44/42 MAPK (Erk1/2; Cell Signaling Technology 9107), and β -Tubulin (Cell Signaling Technology 86298).

Fluorescence imaging of PAGER localization and secondary messenger reporters

Confocal imaging was performed on a Zeiss AxioObserver inverted confocal microscope with 10 \times and 20 \times air objectives, and 40 \times and 63 \times oil-immersion objectives, outfitted with a Yokogawa spinning disk confocal head, a Quad-band notch dichroic mirror (405/488/568/647), and 405 (diode), 491 (DPSS), 561 (DPSS) and 640 nm (diode) lasers (all 50 mW). The following combinations of laser excitation and emission filters were used for various fluorophores: GFP (491 laser excitation; 528/38 emission), mCherry/Alexa Fluor 568 (561 laser excitation; 617/73 emission), Alexa Fluor 647 (647 excitation; 680/30 emission), and differential interference contrast. Acquisition times ranged from 100 to 500 ms. All images were collected using SlideBook (Intelligent Imaging Innovations) and processed using Fiji/ImageJ.

Immunofluorescence staining of PAGER localization

HEK 293T cells expressing the indicated PAGER_{TR} or PAGER_G construct were fixed in 4% paraformaldehyde for 10 min at room temperature, followed by membrane permeabilization by treating with 0.5% Triton-X in PBS for 10 min. The cells were then incubated in 0.1% Tween-20 in PBS supplemented with 1% BSA for 30 min for blocking, followed by 1:1,000 anti-ALFA–AlexaFluor647 in blocking buffer for 1 h to stain for PAGER localization. After three washes in 0.1% Tween-20 in PBS, 1 μ g ml⁻¹ DAPI in PBS was added as a nuclear marker, and the cells were analysed by confocal microscopy.

Fluorescent DAG assay

An mCherry-based fluorescent DAG biosensor was made by C-terminally tagging mCherry to the C1_{PKC γ} from Addgene plasmid #21205³² and cloning into the pCDH lentivirus backbone. HEK 293T cells stably co-expressing anti-GFP (LaG16) PAGER_{Gq} and C1_{PKC γ} -mCherry were incubated in 1:1,000 anti-ALFA–AlexaFluor647 and 1 μ M EGFP for 3 min. Cells were then located under the microscope and time-lapse images were obtained every 4 s, and 1 ml of 150 nM CNO was added (to a final concentration of 100 nM) between the first and the second frame. Images at the first time frame ($t = 0$) and 15th time frame ($t = 60$ s) were used for analysis.

Images were analysed using Fiji/ImageJ software. Regions of interest (ROIs) were manually added to images and the difference in mean of cytosolic mCherry fluorescence ($\Delta(F - F_0)/F_0$) in each cell was quantified to plot the time course of C1_{PKC γ} -mCherry signal. Note: cytosolic mCherry fluorescence was used as a readout for the depletion of DAG probe from cytosol upon membrane recruitment.

GCaMP6s calcium assay

A GFP-based fluorescent calcium biosensor was made by cloning GCaMP6s from Addgene plasmid #40753³³ into the pCDH lentivirus backbone. HEK 293T cells stably co-expressing anti-mCherry (LaM6) PAGER_{Gq} and GCaMP6s were equilibrated in HBSS (Gibco; HBSS, calcium, magnesium, no phenol red) for 10 min at room temperature. Cells were then placed in 500 μ l of HBSS (with or without 1 μ M mCherry) and located under the microscope. Time-lapse images were obtained every 10 s, and 1 ml of CNO or DCZ was added (to a final concentration of 0.3–100 nM) at $t = 30$ s.

Images were analysed using Fiji/ImageJ software. ROIs were manually added to images and the difference in mean of cytosolic GFP fluorescence ($\Delta(F - F_0)/F_0$) in each cell was quantified to plot the time course of GCaMP6s signal. The maximum difference at each DCZ concentration was calculated to obtain dose–response curves.

G-Flamp2 cAMP assay

A GFP-based fluorescent cAMP biosensor was made by cloning G-Flamp2 from Addgene plasmid #192782³⁴ into the pCDH lentivirus backbone. For PAGER_{Gs}, HEK 293T cells stably expressing G-Flamp2 and anti-mCherry (LaM6) PAGER_{Gs} were equilibrated in HBSS (Gibco; HBSS,

Article

calcium, magnesium, no phenol red) for 10 min at room temperature. Cells were then placed in 500 μ l of HBSS (with or without 1 μ M mCherry) and located under the microscope. Time-lapse images were obtained every 10 s, and 1 ml of CNO or DCZ was added (to a final concentration of 0.3–100 nM) at $t = 30$ s.

For PAGER_{G_i}, HEK 293T cells stably expressing G-Flamp2 and anti-mCherry (LaM6) PAGER_{G_i} were equilibrated in HBSS (Gibco; HBSS, calcium, magnesium, no phenol red) for 10 min at room temperature. Cells were then placed in 500 μ l of HBSS (with or without 1 μ M mCherry) and located under the microscope. Time-lapse images were obtained every 10 s, and 500 μ l of 2 μ M forskolin was added (to a final concentration of 1 μ M) at $t = 20$ s, followed by 1 ml of CNO or DCZ (to a final concentration of 0.3–100 nM) at $t = 120$ s.

Images were analysed using Fiji/ImageJ software. ROIs were manually added to images and the difference in mean of cytosolic GFP fluorescence ($\Delta(F - F_0)/F_0$ for PAGER_{G_s}, $\Delta(F - F_{\max})/F_{\max}$ for PAGER_{G_i}, where F_{\max} is a maximum signal upon forskolin stimulation) in each cell was quantified to plot the time course of G-Flamp2 signal. The maximum difference at each DCZ concentration was calculated to obtain dose-response curves.

AAV1/2 generation

To generate supernatant AAV, HEK293T cells were cultured in 6-well plate and transfected at approximately 80% confluency in opti-MEM reduced serum medium (Gibco). Per each well, the AAV vector containing the gene of interest (360 ng) and AAV packaging/helper plasmids AAV1 (180 ng), AAV2 (180 ng), and DF6 (720 ng) incubated with 10 μ l PEI in 200 μ l opti-MEM were used for transfection. After 20 h, the cell medium was replaced with complete DMEM. The cell medium containing the AAV was collected 48 h post transfection and filtered using a 0.45- μ m filter. For in vivo expression, AAV1/2 was produced in a large scale (3 \times 15-cm plates) accordingly and purified using a HiTrap heparin column (GE Healthcare) as previously described⁵⁶.

GCaMP6s neuronal activity assay

All procedures were approved and carried out in compliance with the Stanford University Administrative Panel on Laboratory Animal Care, and all experiments were performed in accordance with relevant guidelines and regulations. Before dissection, 35 mm glass bottom dishes (CellVis) were coated with 0.001% (w/v) poly-L-ornithine (Sigma-Aldrich) in DPBS (Gibco) at room temperature overnight, washed three times with DPBS, and subsequently coated with 5 μ g ml⁻¹ of mouse laminin (Gibco) in DPBS at 37 °C overnight. Cortical neurons were extracted from embryonic day 18 Sprague Dawley rat embryos (Charles River Laboratories, strain 400) by dissociation in Hank's balanced salt solution with calcium and magnesium (Gibco). Cortical tissue was digested in papain according to the manufacturer's protocol (Worthington), then 5 \times 10⁵ cells were plated onto each dish in neuronal culture medium at 37 °C under 5% CO₂. The neuronal culture medium is neurobasal (Gibco) supplemented with 2% (v/v) B27 supplement (Life Technologies), 0.5% (v/v) fetal bovine serum, 1% (v/v) GlutaMAX, 1% (v/v) penicillin-streptomycin, and 1% (v/v) sodium pyruvate (Gibco, 100 mM).

On division 3 and division 6, half of the medium was removed from each dish and replaced with neuronal culture medium. On division 6 after the medium change, each well was infected with 35 μ l of AAV1/2 (10 μ l of GCaMP6s AAV and 25 μ l of anti-mCherry (LaM6) PAGER_{G_i} AAV). Neurons were wrapped in aluminum foil and allowed to express in the incubator.

For HEK–neuron coculture experiments, HEK 293T cells were plated in a 6-well plate and transfected with surface mCherry on a day before the imaging. 8 h after transfection, the HEK cells were collected in PBS without using trypsin. The cells were pelleted and resuspended in neuron culture medium supplemented with 2.5 μ M cytosine β -D-arabinofuranoside hydrochloride (AraC; Sigma-Aldrich C6645).

HEK cells were resuspended at 5 \times 10⁵ cells per ml (for 1:2 HEK:neuron co-culture) or 1 \times 10⁵ cells per ml (for 1:10 HEK:neuron co-culture). Five-hundred microlitres of the resuspended cells were plated on each neuron-plated imaging dish (2 ml culture medium) to make the final AraC concentration 0.5 μ M.

On division 13, cells were preincubated in HBSS for 10 min, and then incubated in 1:1,000 anti-ALFA–AlexaFluor647 and 1 μ M mCherry in HBSS for 3 min. Cells were then located under the microscope and time-lapse images were obtained every 1 s, and 1 ml of 50 nM CNO or 3 nM DCZ was added (to a final concentration of 33 nM or 2 nM) at $t = 10$ s.

Images were analysed using Fiji/ImageJ software. ROIs were manually added to images and the mean of cytosolic GFP fluorescence in each cell was quantified to plot the time course of GCaMP6s signal in the form of $\Delta(F - F_{\min})/(F_{\max} - F_{\min})$.

Neuronal electrophysiology assay in brain slices

Subjects. Adult female C57BL/6 mice (Jackson Laboratory) were used for slice electrophysiology experiments. All procedures were carried out in accordance with the National Institutes of Health guidelines for animal care and use, and were approved by the Administrative Panel on Laboratory Animal Care of Stanford University (protocol 30183). Mice were group housed (2–5 per cage), received ad libitum access to food and water, and were maintained on a 12 h light/dark cycle throughout the study under standard housing conditions (21 \pm 2 °C; 50 \pm 15% humidity).

Slice electrophysiology. Mice received a stereotaxic injection bilaterally into CA1 (M/L: \pm 1.5; A/P: -2.3 ; D/V: -1.35 mm) when 4–8 weeks old of 400 nL AAV1/2 vector containing an hSyn- α -mCherry-PAGER-G_i-P2A-mEGFP expression cassette (1.9 \times 10¹³ genome copies (GC) ml⁻¹). At 3–6 weeks following initial injection, mice were deeply anaesthetized by ketamine/xylazine and then transcardially perfused with an ice-cold protective recovery solution containing (in mM): 92 N-methyl-D-glucamine (NMDG), 26 NaHCO₃, 25 glucose, 20 HEPES, 10 MgSO₄, 5 sodium ascorbate, 3 sodium pyruvate, 2.5 KCl, 2 thio-urea, 1.25 NaH₂PO₄, 0.5 CaCl₂, titrated to a pH of 7.3–7.4 with HCl⁵⁷. Hippocampus-containing coronal brain slices (250 μ m) were cut in ice-cold protective recovery solution using a vibratome (VT1200S, Leica Biosystems) and then incubated in 35 °C protective recovery solution for 12 min. Subsequently, brain slices were maintained in room temperature artificial cerebrospinal fluid (aCSF) consisting of (in mM): 126 NaCl, 26 NaHCO₃, 10 glucose, 2.5 KCl, 2 MgCl₂, 2 CaCl₂, 1.25 NaH₂PO₄. All solutions were equilibrated with 95% O₂/5% CO₂.

Intracellular recordings were performed in a submerged chamber perfused with oxygenated aCSF at 3 ml min⁻¹ and maintained at 33 °C by a chamber heater (BadController V, Luigs and Neumann). CA1 neurons were visualized using differential interference contrast illumination on an Olympus BX61WI microscope (Olympus Microscopy) with an sCMOS camera (Flash 4.0 LT+, Hamamatsu). Epifluorescence illumination from an LED lamp (Solis-3C, Thorlabs) was used to identify GFP-positive transfected neurons. Recording pipettes were pulled from thin-walled borosilicate capillary glass (King Precision Glass) using a P97 puller (Sutter Instruments) and were filled with (in mM): 126 potassium gluconate, 10 HEPES, 4 KCl, 4 ATP-Mg, 0.3 GTP-Na, 10 phosphocreatine (pH-adjusted to 7.3 with KOH, osmolarity 290 mOsm), as well as 0.2% biocytin. Pipettes had a 3–5 M Ω tip resistance.

Whole-cell recordings were performed on GFP-positive CA1 neurons in the dorsal hippocampus (A/P: -1.7 – 2.6 mm). Pipette capacitance was neutralized for all recordings and holding current was adjusted so that all cells began recordings with an initial membrane potential of -65 mV. Neuronal properties were assessed longitudinally, across 5 s sweeps, featuring repeated current injection patterns including a brief hyperpolarizing current step (-100 pA, 200 ms), followed shortly later (300 ms) by a linearly ramping current delivery (-150 to $+500$ pA,

across 2 s). Input resistance (R_{in}) was calculated from the change in steady-state membrane potential resulting from hyperpolarizing current injections. RMP was measured as the average value during the period (500 ms) in each sweep prior to any current injection. All action potentials were counted during the ramping current delivery and the rheobase value was the current being delivered when the first action potential of each sweep was evoked.

At the end of recordings, brain slices were fixed in 4% paraformaldehyde with 0.2% picric acid in 0.1 M phosphate buffer for 24 h at 4 °C. Biocytin-filled neurons were labelled by washing sections in PBS, permeabilizing with 0.5% Triton X-100 (Sigma-Aldrich) in TBS and then overnight incubation at 4 °C in Alexa Fluor 405-conjugated streptavidin (1:1,000, Molecular Probes). Sections were then washed and mounted in Vectashield (Vector Laboratories), before collecting z-stack images of the biocytin and mEGFP signals in the hippocampus using a Zeiss LSM 710 confocal microscope using a 20× 0.8 NA objective.

Data were excluded from cells where the initial R_{in} was >500 mΩ, as well as individual sweeps where the RMP was >-50 mV or where no action potentials were detected. Responses were tracked during bath application of DCZ (100 nM, Tocris) or the same dose of DCZ combined with soluble mCherry (1 μM). All cells recorded with DCZ + mCherry also underwent a prior preincubation in mCherry (1 μM; range: 30–150 min, mean: 73.4 min). Recordings in DCZ alone were avoided after >1 DCZ + mCherry experiment per day to reduce potential cross contamination. Data were collected from $n = 15$ cells, 7 mice with DCZ, $n = 26$ cell, 6 mice DCZ + mCherry. Recordings were only performed in brain slices naïve to prior DCZ exposures. Data were acquired in pClamp software (Molecular Devices) using a Multiclamp 700B amplifier (Molecular Devices), low-pass filtered at 2 kHz, and digitized at 10 kHz (Digidata 1440 A, Molecular Devices). Data analysis was performed using custom written Python scripts.

Statistical analysis. Graphs and statistical analyses were generated using Python (with Pandas, Seaborn, Scipy and Statsmodels packages). To account for the nested data produced in whole-cell electrophysiology experiments where multiple cells are recorded from each animal, differences between treatment groups were evaluated by a mixed linear model regression analysis⁵⁸. Sex was not considered in the current study design and a sex-based analysis was not performed, with our current data being restricted entirely to female samples. Analysis of neuronal responses was conducted blinded to treatment groups.

Lentiviral transduction of primary human T cells

On day 0, primary human T cells were thawed and activated with anti-CD3/CD28 human T-Expander Dynabeads (Thermo Fisher Scientific) at a 1:1 bead to cell ratio. On day 2, 1 ml of 500,000 cells per ml T cell suspension was added to each well of a 24-well non-tissue culture treated plate. To each well, 1.6 μl of 10 mg ml⁻¹ polybrene (for 8 μg ml⁻¹ in 2 ml final) was added to each well. One millilitre of lentivirus was added per well. Plates with T cell/virus mixes were spun at 1,000g for 2 h at 32 °C in an aerosol tight plate holder. After the 2 h spin, cells were resuspended, moved to 6-well plates, and incubated for 24 h at 37 °C under 5% CO₂. On day 4, Dynabeads were removed by magnetic separation and lentivirus was removed by centrifugation. Cells were maintained between 0.4×10^6 and 2×10^6 cells per ml and expanded until day 11–12. On day 11–12, PAGER-expressing T cells were enriched by magnetic-activated cell sorting (MACS; using an ALFA–biotin antibody (NanoTag) and ALFA–biotin antibody (NanoTagbiotin microbeads (Miltenyi)) or by fluorescent-activated cell sorting (FACS; using ALFA-647 antibody (NanoTag)). Typically, enriched T cells were >95% PAGER⁺. PAGER⁺ T cells were used for experiments on days 14–19.

T cell migration assays

In a 96-well Transwell plate (3 μm pore size; Corning), 80 μl of 1.25×10^6 PAGER⁺ T cells ml⁻¹ (~100,000 cells) were plated in the top chamber.

T cells were let to settle for 1 h at 37 °C under 5% CO₂. After 1 h, 0.8 μl 100 nM DCZ was added to the top chamber of each well and 240 μl of medium containing 1 nM DCZ and cognate (10 μM mCherry) or non-cognate (10 μM GFP) antigen was added to the bottom chamber of each well. This way, the DCZ concentration was equal across the entire well (that is, no DCZ gradient formed) and only a gradient of antigen (mCherry or GFP) was formed over time. T cells were incubated at 37 °C under 5% CO₂ for 2 h to let chemotaxis migration to occur. For experiments where pertussis toxin (PTX) was used to assess the role of G_i activation in PAGER-mediated chemotaxis, after PAGER⁺ T cells were added to the top chamber of each well, 1 μl of 16 μg ml⁻¹ PTX was added to the cells (final 200 ng ml⁻¹ PTX) and let incubate at 37 °C under 5% CO₂ for 3 h before adding DCZ/antigen-containing medium in the bottom chambers. For time course experiments, separate wells were set up for each time point and DCZ/antigen-containing medium was added to the bottom chambers at different times so all wells could be collected together.

After incubation for 2 h to allow for chemotaxis, T cells that migrated from the top chamber, across the porous membrane, to the bottom chamber were collected; all of the medium in the bottom chamber (~240 μl) was moved to wells of a 96-well v-bottom plate and the centrifuged in swinging bucket rotor at 1,000g for 5 min. Medium in the wells was removed by flicking off and dabbing excess on paper towel. One-hundred microlitres DPBS was added to each well of the 96-well v-bottom plate and pipetted up and down 10 times to resuspend any potential T cells in the wells. This cell suspension was then moved to a white 96-well solid-bottom plate where CellTiter-Glo 2.0 was used to create a luminescent signal proportional to the number of T cells present. 100 μl of CellTiter-Glo 2.0 was added to each well and mixed by hand for 1 min, let incubate for 10 min at room temperature in the dark, and then luminescence was measured using a Tecan Infinite M1000 Pro plate reader using the following parameters: 1,000 ms acquisition time, green-1 filter (520–570 nm), 25 °C linear shaking for 10 s. Schematic summary of T cell migration assay was created, in part, using BioRender.

The development of GRAB_{DCZ} sensors

We chose human M4R as the sensor scaffold and embarked on a systematic optimization process. This process included screening and optimizing the insertion sites, the amino acid composition of the linker, and the critical residues in cpEGFP to enhance the maximum response and fluorescence of sensors. Subsequently, specific DCZ sensors were developed by introducing binding pocket mutations based on these sensors.

- ICL3 replacement: we replaced the ICL3–cpEGFP of the previously developed GRAB_{gACh} sensor¹ with the corresponding ICL3 of hM4R. A replacement library was generated using 9 sites (S5.62 to H5.70) from the N terminus and 5 sites (T6.34 to F6.38) from the C terminus. After screening, we created a prototype ACh sensor named hM4-0.1, which exhibited a 100% ΔF/F fluorescence response to 100 μM ACh. The replacement sites of hM4-0.1 are located between R5.66 and T6.36 in hH4R.
- Linker optimization: the amino acid composition of the linker was found to be critical to the sensor's dynamic range. We performed site-saturation mutagenesis on 6 residues of the linker. Through this process, we identified a variant named hM4-0.5, with an R5.66 L mutation, which resulted in a ~130% increase in ΔF/F₀.
- cpEGFP optimization: building on our screening experience in developing GRAB sensors^{2,3}, we selected four residues in the cpEGFP for individual randomizations. This led to the development of the hM4-1.0 sensor with an H18I mutation, showing a maximal response of ~350% to 100 μM ACh.
- Binding pocket mutations: to develop specific DCZ sensors, we introduced Y3.33 C and A5.46 G mutations^{11,59} based on the hM4-1.0, resulting in the creation of DCZ1.0, which exhibited a ~150% response to 1 μM DCZ.

Fluorescence imaging of GRAB sensors and PAGER_{FL}

The Opera Phenix high-content screening system (PerkinElmer) was utilized for GRAB sensors and PAGER_{FL} imaging, equipped with a 20× 0.4-NA objective, a 40× 0.6-NA objective, a 40× 1.15-NA water-immersion objective, a 488-nm laser, and a 561-nm laser. GFP and RFP signals were collected using a 525/50 nm emission filter and a 600/30 nm emission filter, respectively. HEK293T cells expressing GRAB_{DCZ1.0} or PAGER_{FL} were imaged before and after adding specified DCZ/antigens while being bathed in Tyrode's solution. The change in fluorescence intensity of GRAB_{DCZ1.0} was determined by calculating the change in the GFP/RFP ratio and expressed as $\Delta F/F_0$, F_0 is the intensity of sensors in the basal (no DCZ/antigen) condition.

Mini G-protein luciferase complementation assay

HEK293T cells were cultured in 6-well plates until they reached 60–70% confluence. At this point, the specified wild-type receptor or sensor, along with the corresponding LgBit-mG_i construct, were co-transfected into the cells. Around 24–36 h post-transfection, the cells were detached using a cell scraper, suspended in PBS, and then transferred to 96-well plates (white with a clear flat bottom) containing Nano-Glo Luciferase Assay Reagent (Promega) diluted 1,000-fold in PBS at room temperature. Following this, solutions with varying DCZ concentrations and 1 μ M antigens were added to the wells. After a 10-min reaction in the dark at room temperature, luminescence was measured using a VICTOR X5 multi-label plate reader (PerkinElmer).

Quantification and Data Analysis

All graphs were created using GraphPad Prism 9 or matplotlib (Python). Error bars represent s.d. unless otherwise noted. For scatter plots, variable slope (four parameter) non-linear regression lines were used. For comparison between two groups, *P* values were determined using two-tailed Student's *t*-tests. For multiple comparisons, *P* values were determined using two-way ANOVA with Tukey's multiple comparisons test to adjust for multiple comparisons. **P* < 0.05; ***P* < 0.01; ****P* < 0.001; *****P* < 0.0001; NS, not significant.

General guidelines for designing and validating PAGERS

A workflow for developing and optimizing new PAGERS is outlined below. These steps are generally the same no matter which type of PAGER (PAGER_{TF}, PAGER_G, or PAGER_{FL}) is being developed, but specific notes and tips for the creation of different types of PAGERS are also included.

Choosing an antigen binding domain. The specificity and sensitivity of a given PAGER is primarily determined by the antigen binding domain that is used. If available, we recommend using a nanobody for the antigen binding domain, as we have had the most success building functional PAGERS with this class of binder; ~50% of all nanobodies tested resulted in functional PAGERS. Other binding domains that have their N terminus proximal to the binding interface may also work. When possible, we suggest starting with 2–3 high-affinity binders against your antigen of interest to test in PAGER, as the affinity of binders for antigen in the context of PAGER may be different (oftentimes lower) than their published affinities.

Construct design. The relative position of the binder and the antagonist is critical. The antagonist should be fused directly to the N terminus of the binder (no linker between). This is because proximity of the antagonist to the CDR loops of the binder creates the steric occlusion of the antagonist upon antigen binding that is necessary for PAGER activation. Even short linkers between the antagonist and binder may make PAGER insensitive to soluble antigen. In our constructs, we also typically omit the first 2–3 amino acids of the nanobody (for example, MAQ) so as to place the antagonist as near to the nanobody CDRs as possible.

The linker between the binder and the GPCR is less critical but needs to be sufficiently long to allow the antagonist to reach the GPCR active site. This linker is also a convenient location to insert an epitope tag to detect PAGER expression. We generally use ALFA tag due to its small size and non-perturbative helical structure. Importantly, we highly recommend including a TEVcs (ENLYFQ/S) in this linker, as it is useful for assessing antagonism in newly generated PAGER constructs (described in step 3 below).

Signal peptides are included in all PAGER constructs to promote surface expression of the receptor. For PAGER_G and PAGER_{FL}, we use the native signal peptide of muscarinic toxin. PAGER_{TF} requires a signal peptide that does not leave any residues on the N terminus of the antagonist (that is, no P' residues in the cleavage sequence of the signal peptide), as the N-terminal residues of the aro-dyn peptide antagonist in PAGER_{TF} are essential for peptide binding and antagonism. All PAGER_{TF} constructs we developed utilize an IL-2 signal peptide, which does not leave an N-terminal scar, but other scarless signal peptides could also be used.

Screening for expression, localization, and reversible auto-inhibition.

We recommend first screening candidate PAGERS in HEK293T cells before moving to other cell types of interest. We have found that PAGER expression, surface localization, and antagonism are the key features that determine overall PAGER functionality. To assess all these aspects simultaneously, we devised a screen using recombinant TEVp and the extracellular TEVcs discussed in step 2 above. In this approach, a dose–response curve of PAGER agonist (SalB for PAGER_{TF} or DCZ/CNO for PAGER_G/PAGER_{FL}) should be conducted with and without pretreatment with recombinant TEVp (we typically pretreat PAGER-expressing cells with 1 μ M TEV for 90 min, but as little as 30 min is also sufficient). In the absence of TEVp, a dose-dependent activation of PAGER should be observed, as increasing concentrations of agonist will outcompete the fused antagonist and activate the receptor; this alone confirms whether the PAGER is expressed and activatable. With TEVp pretreatment, the antagonist should be cleaved, sensitizing the PAGER to the agonist, and result in the dose–response curve shifting to the left; this confirms surface localization (since the recombinant TEVp can only act on plasma membrane localized PAGERS) and reversible antagonism. As further validation, immunofluorescence and flow cytometry should be conducted to confirm PAGER expression and surface localization.

In our experience, any PAGER that fails this TEV test (that is, does not show a clear dose–response curve with a leftward shift upon TEVp pretreatment) has also been unresponsive to antigen. Furthermore, 83% of PAGERS that passed this test went on to be responsive to antigen. Therefore, this screen is a simple intermediate step to save time and resources by narrowing the list of candidate PAGERS to those with a high likelihood of success prior to antigen screening.

Screening for response to antigen. PAGERS that pass the TEVp screen should then be tested using the target antigen. The agonist concentration that yielded the highest signal:noise in the TEV screen (+TEV/–TEV) should be used for antigen testing. We generally recommend performing antigen dose–response curves to determine the overall affinity and sensitivity of each PAGER to the antigen of interest.

Ideally, you might have multiple PAGERS that respond to your antigen of interest. In this case, it is important to consider your downstream application when choosing which PAGER to move forward with. PAGERS with higher affinity binders offer higher sensitivity to the antigen but may also exhibit slow or irreversible antigen binding, while PAGERS with lower-affinity binders typically provide lower sensitivity but higher reversibility, enabling activation only during coincidence detection of antigen and agonist (Sal B or DCZ/CNO). The concentration of antigen that you wish to detect using PAGER should also be considered; to detect higher concentrations of antigen, a low sensitivity PAGER may

suffice, but to detect lower concentrations of antigen, a high sensitivity PAGER may be required. All these factors should guide the selection of a PAGER with characteristics best suited for the user's downstream applications.

Optimization of PAGER expression in a cell type of interest. In our studies, choosing the right promoter for the target cell type was a key factor for successful PAGER expression. For example, CMV promoter worked best in HEK 293T cells while SFFV promoter worked best for T cells. The expression and delivery method also depend on the target cell type. Expression methods commonly used for your cell type of interest are a good starting point, but testing multiple approaches is likely to help identify the best method for optimal PAGER expression. Of note, the larger size of PAGER_{TF} compared to PAGER_G or PAGER_{FL} (-3 kb vs -2 kb) and the two additional gene components of PAGER_{TF} (the arrestin-TEVp and the transcriptional response element) require co-transduction of two or three viruses into the target cells. Combining two PAGER_{TF} components into a single lentivirus may facilitate the reconstitution of all components by requiring one less virus to be co-transduced. As with other multiple component systems, proper relative expression of the components needs to be achieved and often needs to be determined empirically.

Reporting summary

Further information on research design is available in the Nature Portfolio Reporting Summary linked to this article.

Data availability

All data supporting the findings of this study are available within the paper and its Supplementary Information. No separate datasets were generated or analysed for the current study.

Code availability

Custom scripts were developed using a combination of ImageJ macros and Python for automated image intensity calculation and data

processing. The matplotlib library in Python was used for data visualizations. All custom Python scripts used in this study are available upon request.

56. Kim, C. K. et al. A molecular calcium integrator reveals a striatal cell type driving aversion. *Cell* **183**, 2003–2019.e16 (2020).
57. Ting, J. T., Daigle, T. L., Chen, Q. & Feng, G. in *Patch-Clamp Methods and Protocols* (eds Martina, M. & Taverna, S.) 221–242 (Springer, 2014); https://doi.org/10.1007/978-1-4939-1096-0_14.
58. Aarts, E., Verhage, M., Veenvliet, J. V., Dolan, C. V. & van der Sluis, S. A solution to dependency: using multilevel analysis to accommodate nested data. *Nat. Neurosci.* **17**, 491–496 (2014).
59. Zhang, S. et al. Molecular basis for selective activation of DREADD-based chemogenetics. *Nature* **612**, 354–362 (2022).

Acknowledgements The authors are grateful to the St Jude Children's Research Hospital Collaborative Research Consortium on GPCRs, the Chan Zuckerberg Biohub–San Francisco, Phil and Penny Knight Initiative for Brain Resilience (KIG-104), Stanford Cancer Institute, Wu Tsai Neurosciences Institute of Stanford University and the NIH (MH135934 to A.T. and I.S., F32CA257159 to N.A.K., NS121106 to I.S.) for funding this work. Support from the National Natural Science Foundation of China (31925017 to Y.L.) and the New Cornerstone Science Foundation through the New Cornerstone Investigator Program and the XPLOER PRIZE (to Y.L.) is also acknowledged. R.T. was supported by the Life Sciences Research Foundation Fellowship (sponsored by Astellas Pharma) and JSPS Overseas Research Fellowship. The authors thank S. Lee and M. Lin for providing rat cortices; S. Malhotra for assistance with slice electrophysiology preparations; and R. Hernandez-Lopez for helpful discussions and equipment access. Images in Figs. 2b,e and 4 were created with BioRender. We thank Tony Kalogiropoulos for his unwavering guidance, support, encouragement, and inspiration; may his memory be eternal.

Author contributions N.A.K. and A.T. conceived the project. N.A.K. and A.T. designed and characterized PAGER_{TF}. R.T., N.A.K. and A.T. designed and characterized PAGER_G. Y.Y. and Y.L. designed and characterized PAGER_{FL}. M.R. designed the TEVp assay to screen for reversible inhibition of PAGER. The remaining authors contributed to PAGER applications as follows: N.A.K. and B.C. conducted PAGER_{TF} applications; R.T. applied PAGER_G in neuron culture; P.M.K. and I.S. applied PAGER_G in mouse brain; and N.A.K. applied PAGER_G in T cells. N.A.K., R.T. and A.T. wrote the manuscript with input and edits from other authors.

Competing interests N.A.K., A.T., M.R., and R.T. are inventors on a provisional patent (US Provisional Patent Application no.: 63/516,900) related to this work. A.T. is a scientific advisor to Third Rock Ventures and Nereid Therapeutics.

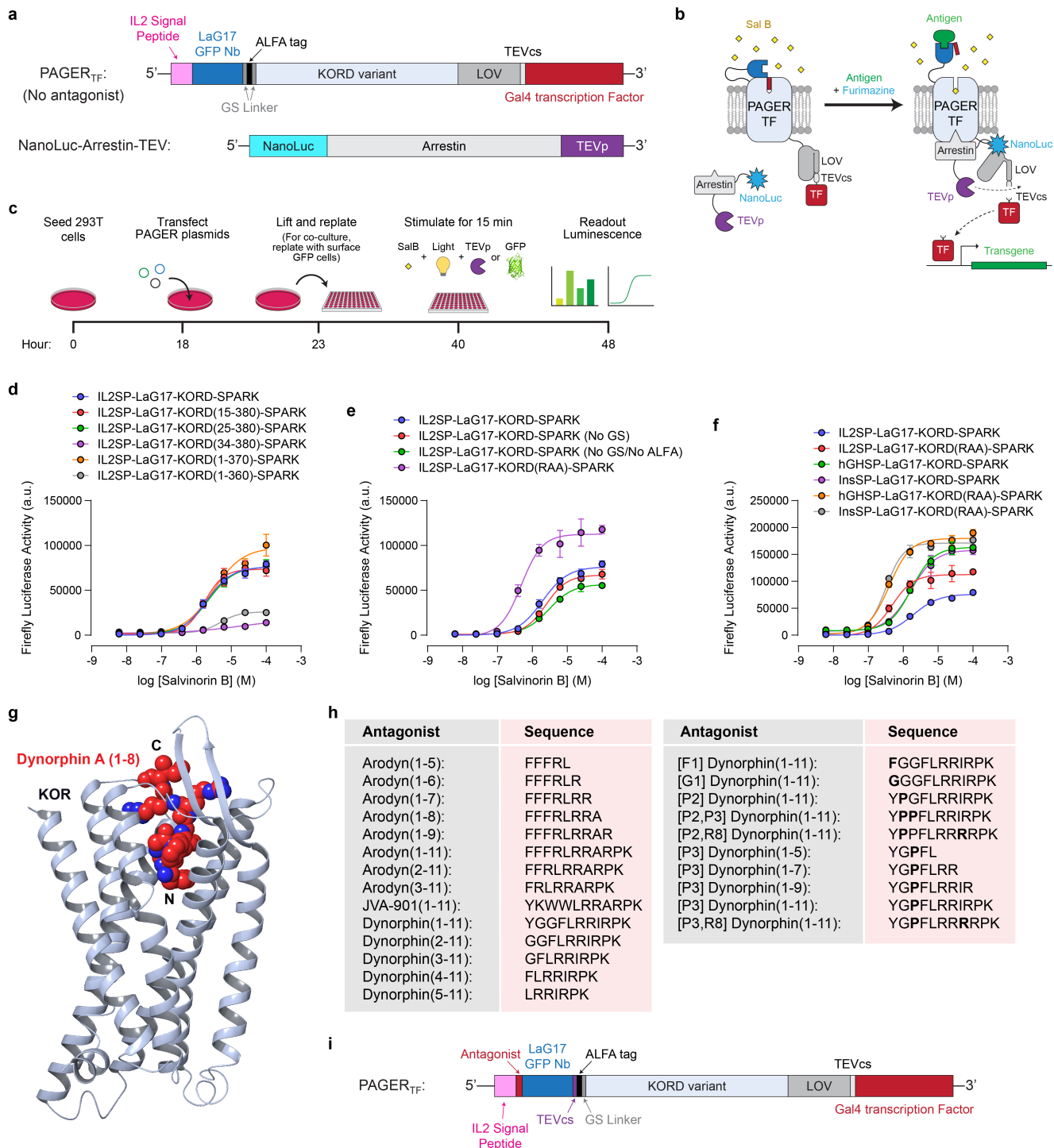
Additional information

Supplementary information The online version contains supplementary material available at <https://doi.org/10.1038/s41586-024-08282-3>.

Correspondence and requests for materials should be addressed to Alice Ting.

Peer review information Nature thanks Bryan Roth, Ofer Yizhar and the other, anonymous, reviewer(s) for their contribution to the peer review of this work.

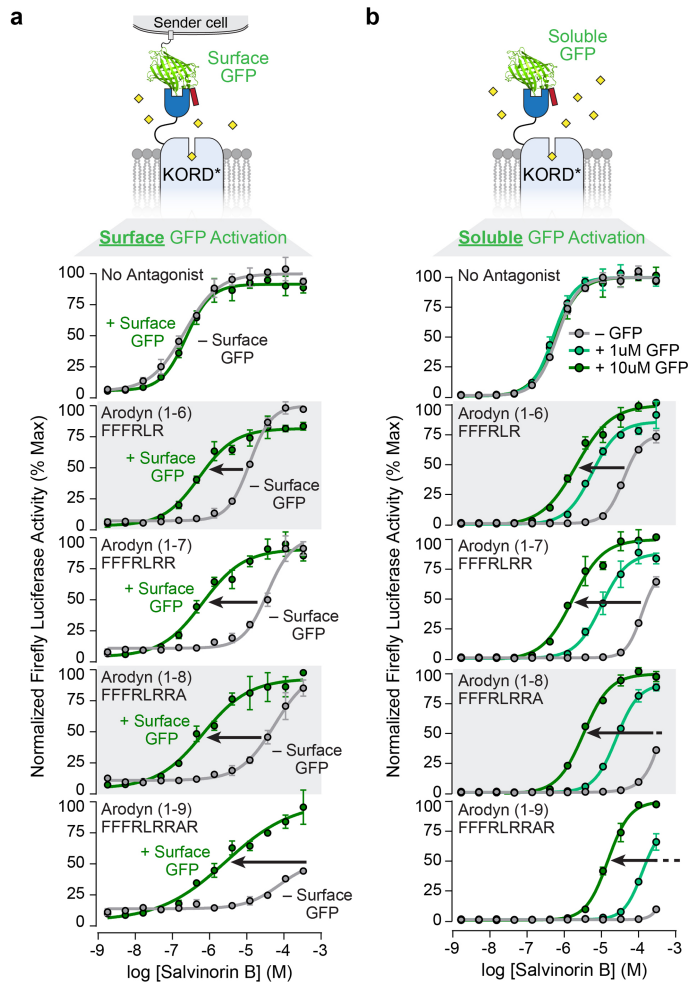
Reprints and permissions information is available at <http://www.nature.com/reprints>.



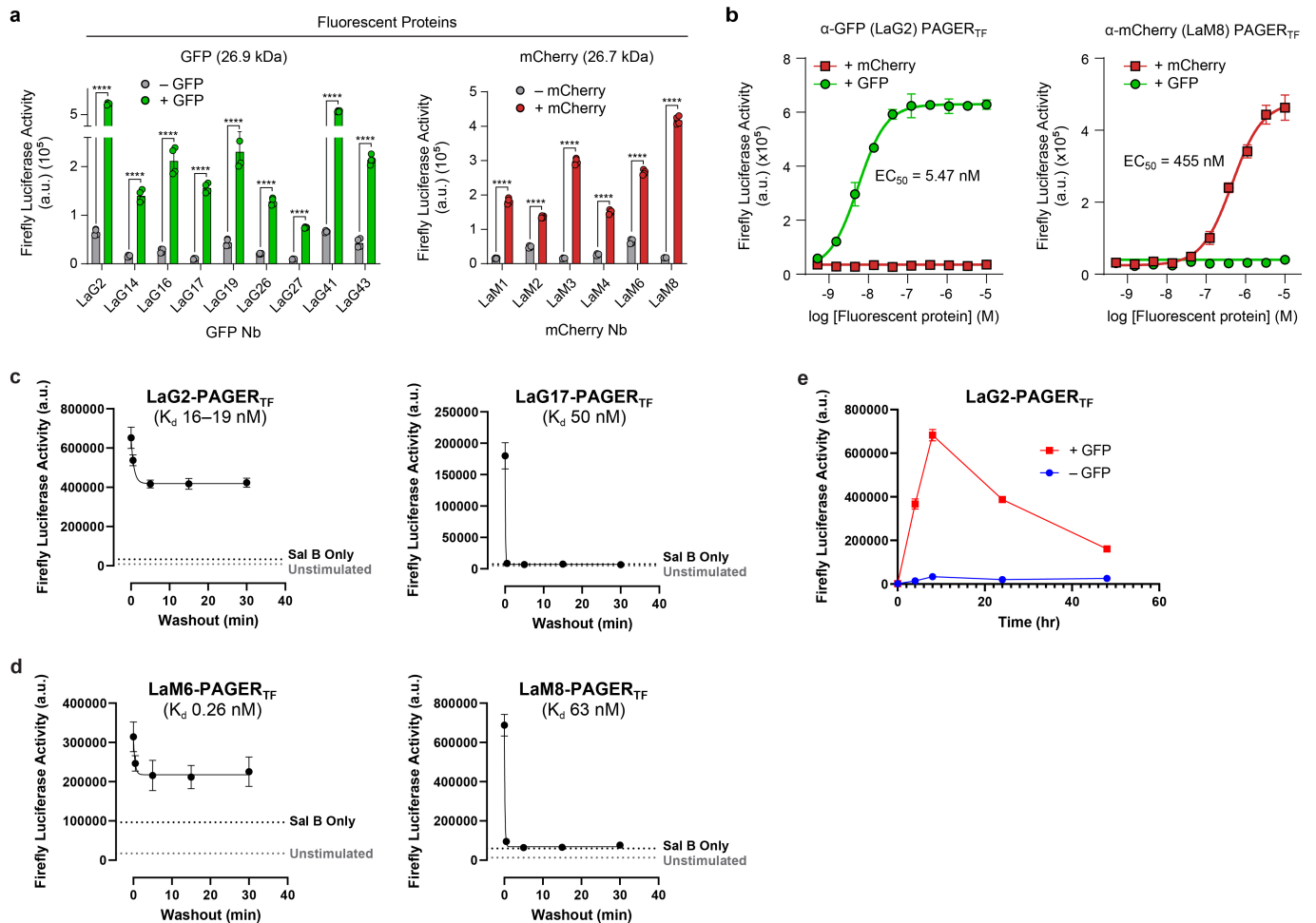
Extended Data Fig. 1 | Domain structure and optimization of PAGERTF.

a, Domain structures of PAGERTF (without antagonist) and Arrestin-TEVp. **b**, Schematic showing how furimazine instead of light can be used to uncage LOV-TEVcs in PAGERTF. This is based on our previous SPARK tools^{14,15}. NanoLuc luciferase fused to arrestin-TEVp is recruited to activated PAGERTF and uncages the LOV domain via BRET when furimazine (NanoLuc's substrate) is present. Uncaging leads to TEVcs cleavage by TEVp and TF translocation to the nucleus. Alternatively, these same PAGERTF constructs can be uncaged using blue light. **c**, Schematic and experimental timeline for PAGERTF assay. **d-f**, Optimization of PAGERTF construct. SalB dose response curves of PAGERTF constructs with various truncations in KORD (**d**), various linkers or RAA mutation in KORD (**e**), and various signal peptides (**f**). RAA refers to V360A/R361A mutations

(-RVR- to -RAA-) in the KORD gene. IL2SP, hGHSP, and InsSP are Interleukin-2 (IL2), human growth hormone (hGH) and insulin signal peptides, respectively. Full length KORD (V360A/R361A) with an IL-2 signal peptide was chosen as the optimal PAGERTF construct and used in all subsequent experiments. Plots are mean \pm s.d. for 3 technical replicates per condition, representing $n = 2$ independent experiments. **g**, Crystal structure of the Kappa-opioid receptor (KOR) in complex with dynorphin A (PDB: 8F7W)¹³. Dynorphin binds KOR with its N-terminus buried in the orthosteric binding pocket. **h**, List of candidate peptide antagonists screened in PAGERTF in Fig. 1c. **i**, Domain structure of α -GFP PAGERTF including an N-terminal antagonist and TEVcs in the extracellular linker between KORD and nanobody.



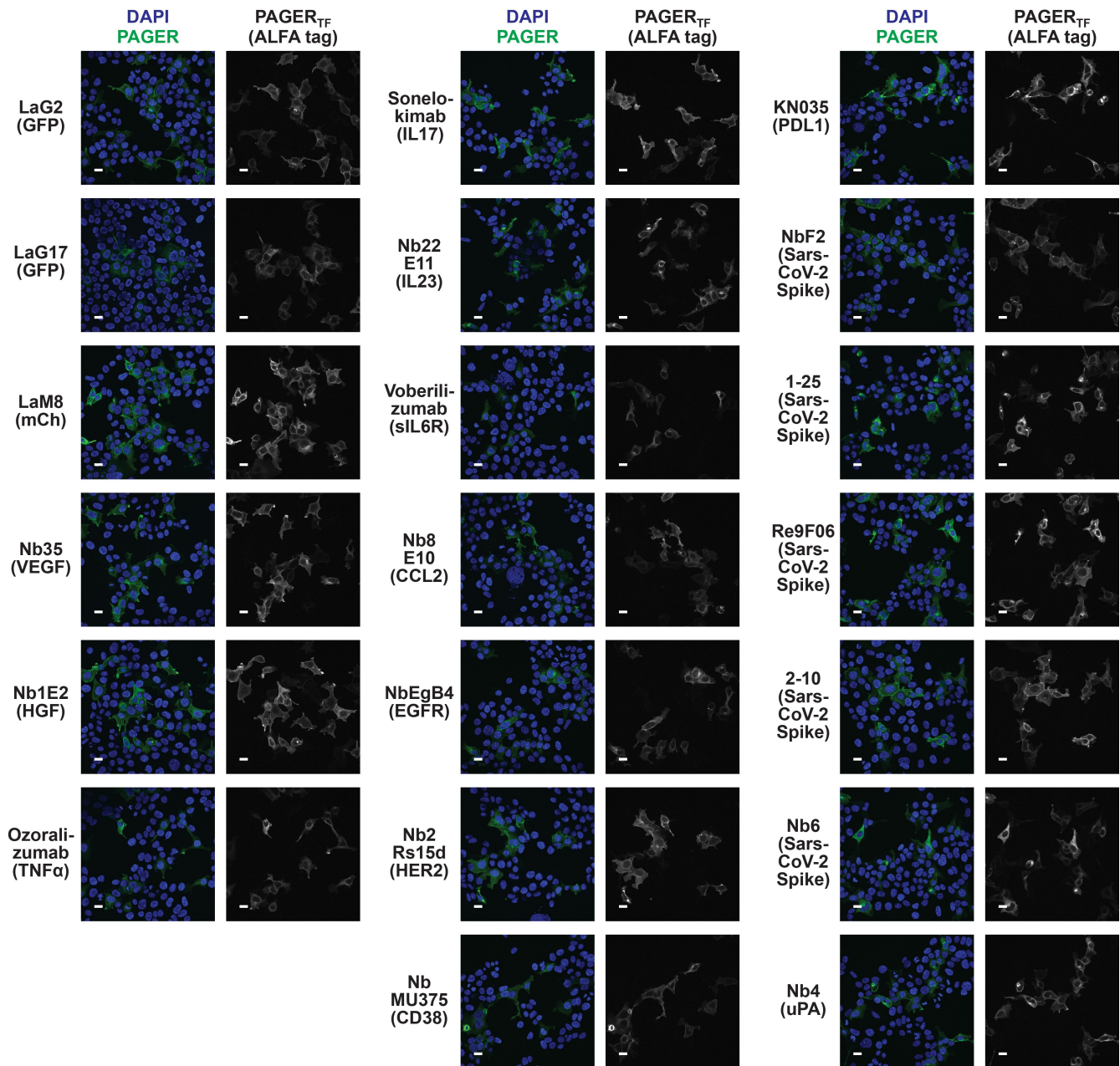
Extended Data Fig. 2 | Testing PAGER_{TF} with different antagonist peptides for response to surface or soluble GFP antigen. a, SalB dose response curves for various PAGER_{TF} constructs with or without co-culture with surface GFP-expressing sender cells. **b**, SalB dose response curves for various PAGER_{TF} constructs with or without soluble GFP. Data presented here shows the same data (normalized) that is shown in Fig. 1k-l (update callouts) but with additional arodyn peptide antagonists included. Plots are mean \pm s.d. for 3 technical replicates per condition, $n = 1$ independent experiment.



Extended Data Fig. 3 | Testing many GFP and mCherry nanobodies in PAGER_{TF}

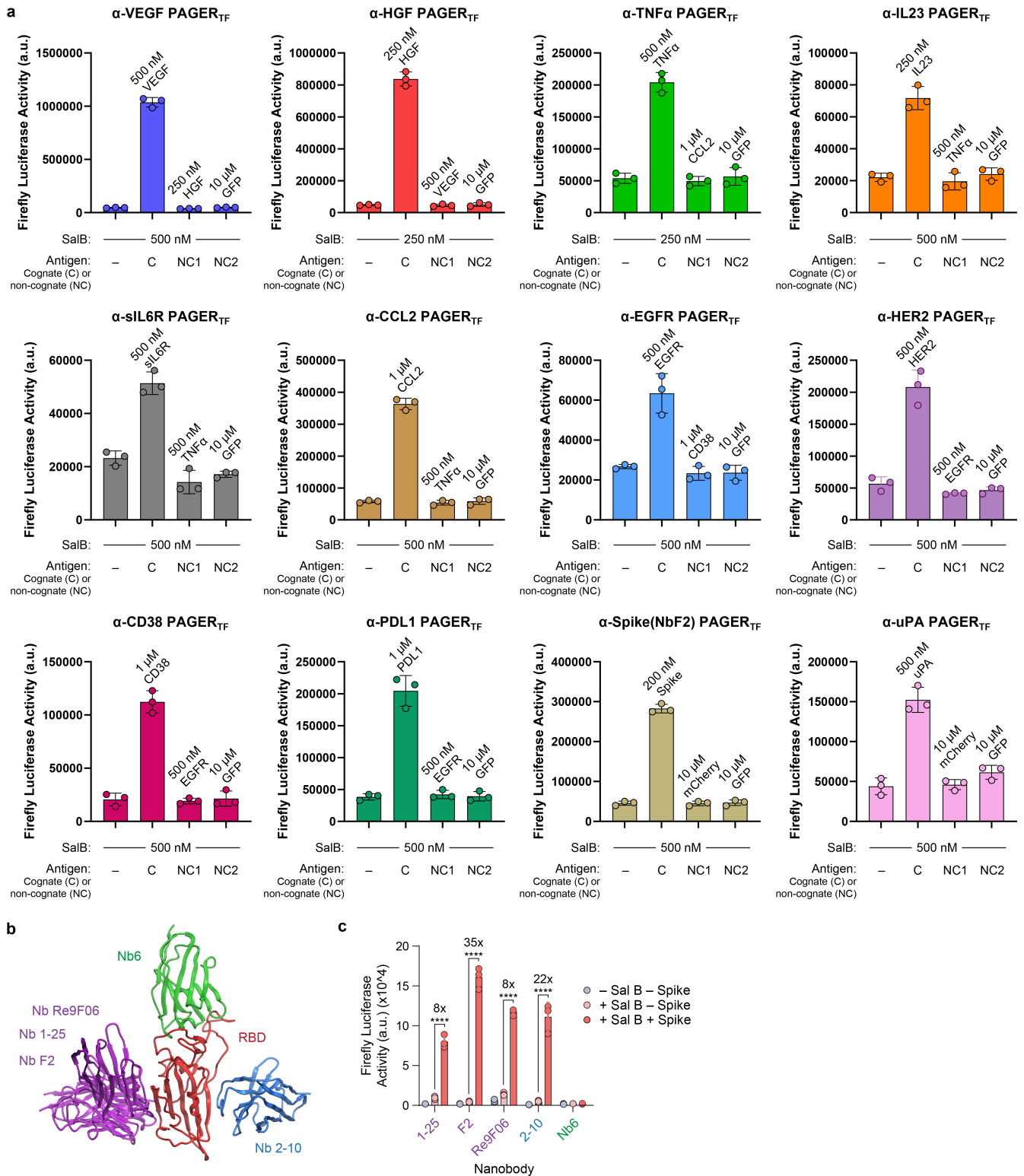
a, Different GFP and mCherry-binding nanobodies work in PAGER. HEK cells expressing PAGER_{TF} with the indicated nanobodies were stimulated with Salvinorin B and 1 μ M soluble GFP or 10 μ M soluble mCherry, for 15 min. Luciferase reporter expression was measured 8 h later. Plots are mean \pm s.d. for 4 technical replicates per condition, representing $n = 3$ independent experiments. p-values were determined using two-tailed Student's t tests. ****, $p < 0.0001$. **b**, mCherry and GFP PAGERs are orthogonal. Data obtained using starved constructs in (a). Plots are mean \pm s.d. for 3 technical replicates per condition, representing $n = 3$ independent experiments. **c–d**, PAGER_{TF} activity as a function of washout time

following 10 μ M soluble GFP (c) or mCherry (d) addition. Washout consisted of incubation in blank DMEM for 0 to 30 min. Cells were then treated with 1 μ M SalB and firefly luciferase reporter activity was measured 8 h later. Control conditions omit antigen (SalB only) or omit SalB (Unstimulated). Plots are mean \pm s.d. for 3 technical replicates per condition, representing $n = 2$ independent experiments. **e**, Time-course of luciferase activity after activation of α -GFP PAGER_{TF} in HEK 293 T cells. Luciferase activity was measured 0–48 h after stimulation with 10 μ M cognate antigen (GFP) and 1 μ M SalB. Plots are mean \pm s.d. for 3 technical replicates per condition, $n = 1$ independent experiment.



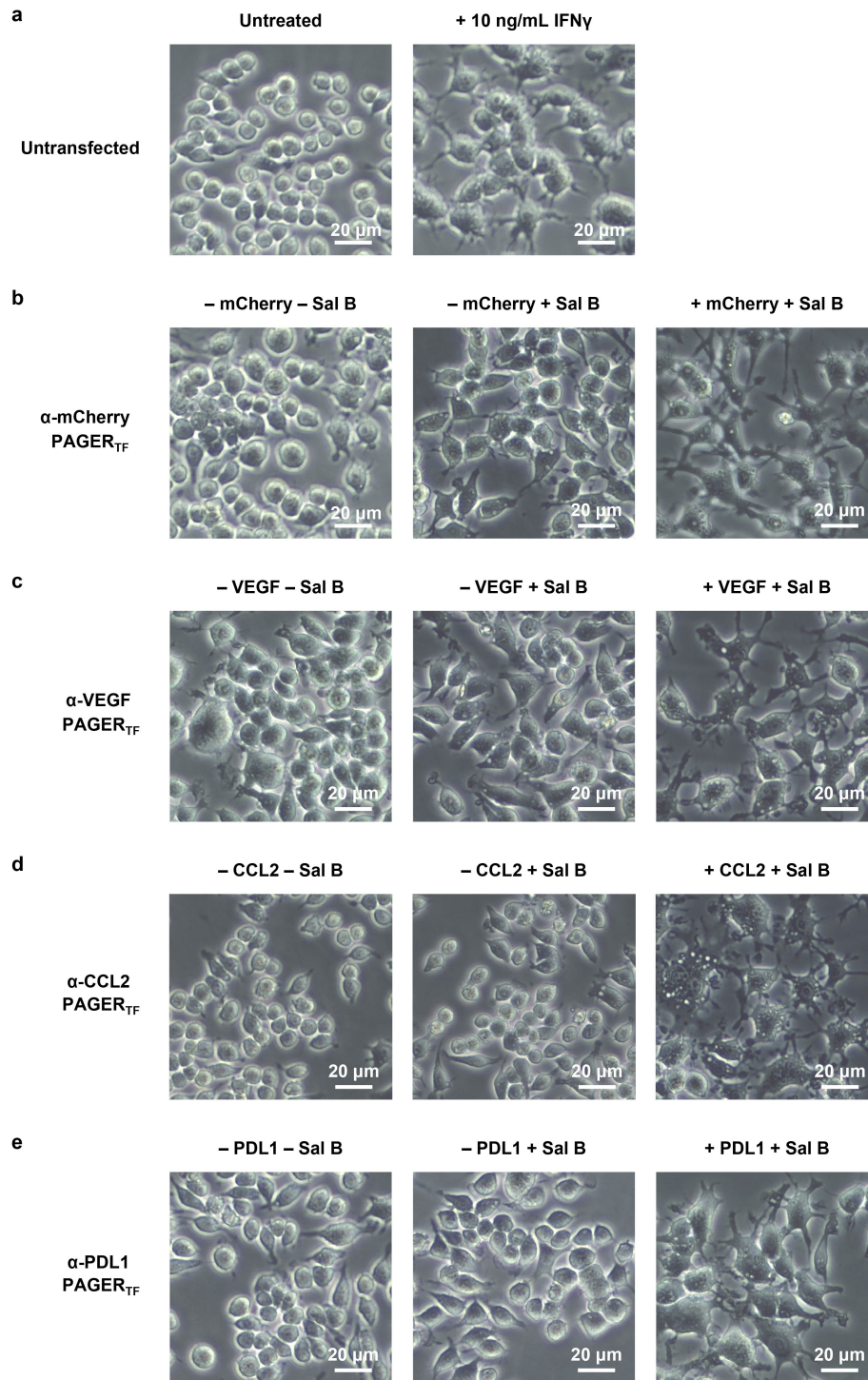
Extended Data Fig. 4 | Imaging PAGER_{TF} expression and membrane localization. Immunofluorescence staining of fixed and permeabilized HEK 293 T cells transiently expressing PAGER_{TF} with the indicated nanobody (target

antigen shown in parentheses), using α-ALFA–Alexa Fluor 647 to detect PAGER (green) and DAPI to stain nuclei (blue). Images are representative of more than three fields of view per condition. Scale bars, 20 μm.



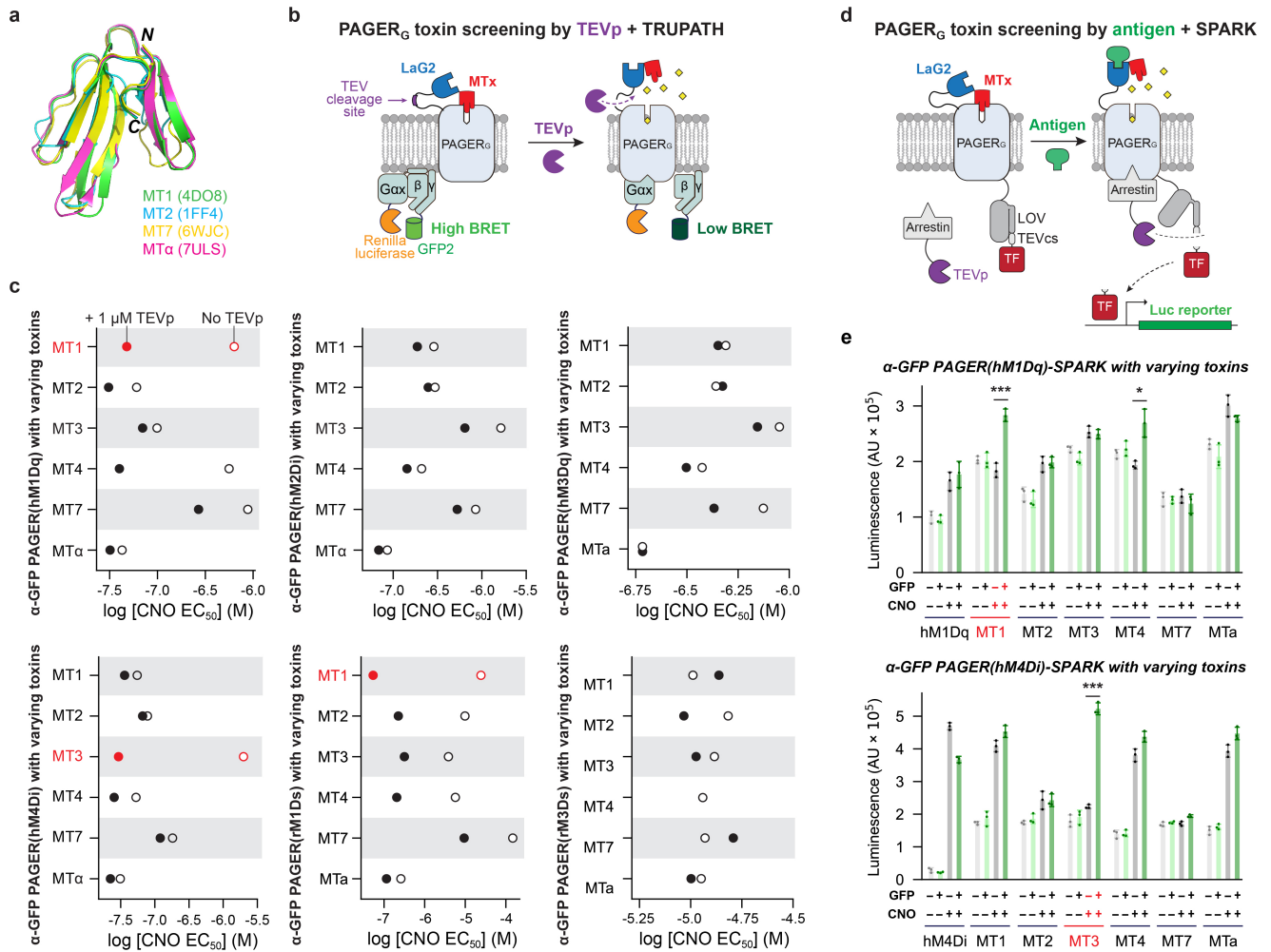
Extended Data Fig. 5 | PAGER_{TF} detects a wide range of antigens (Related to Fig. 2a). **a**, PAGER_{TF} antigen response assay. Same as Fig. 2a, but including comparisons of cognate antigen to two non-cognate antigens for each PAGER_{TF}. The antigens used and their concentrations are labeled above each bar. Plots are mean \pm s.d. for 3 technical replicates per condition, $n = 1$ independent experiment. **b**, Five nanobodies that bind to the receptor binding domain (RBD) of SARS-CoV2 spike protein as shown (sequences in Supplementary Information)

were tested in PAGER_{TF}. **c**, HEK cells expressing the indicated PAGER_{TF} were treated with 200 nM spike protein and 500 nM SalB for 15 min before luciferase measurement 8 h later. Plots are mean \pm s.d. for 3 technical replicates per condition, representing $n = 2$ independent experiment. p-values were determined using two-way ANOVA with Tukey's multiple comparisons test to adjust for multiple comparisons. ****, $p < 0.0001$.



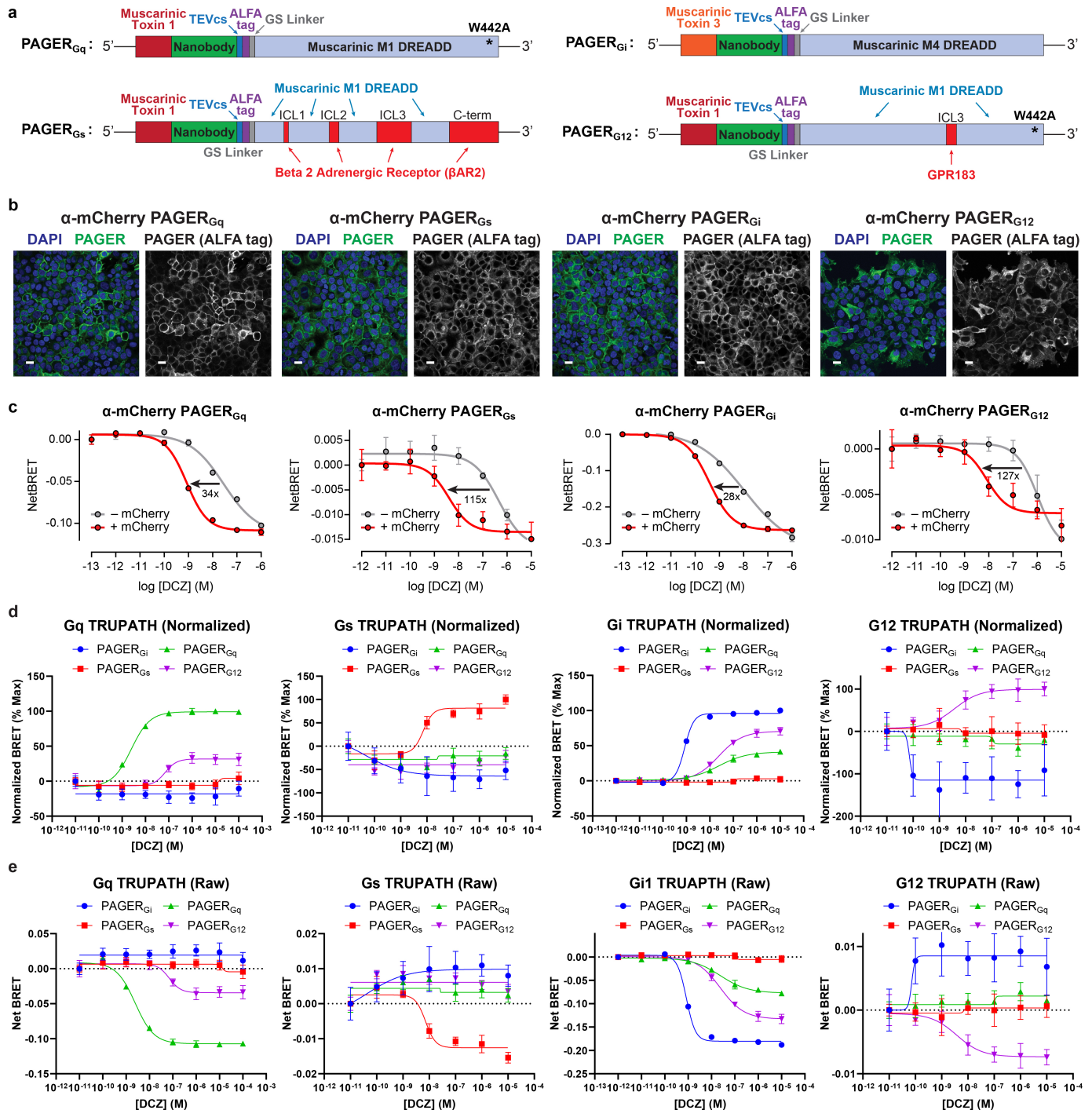
Extended Data Fig. 6 | PAGER_{TF}-induced IFN γ drives macrophage differentiation (Related to Fig. 2b-d). Representative images of Raw 264.7 macrophages after 48 h of co-culture with the indicated PAGER_{TF}-expressing

HEK293T cells. Images are representative of $n = 3$ experiments and are from the same experiment shown in Fig. 2c,d. Scale bars, 20 μ m.



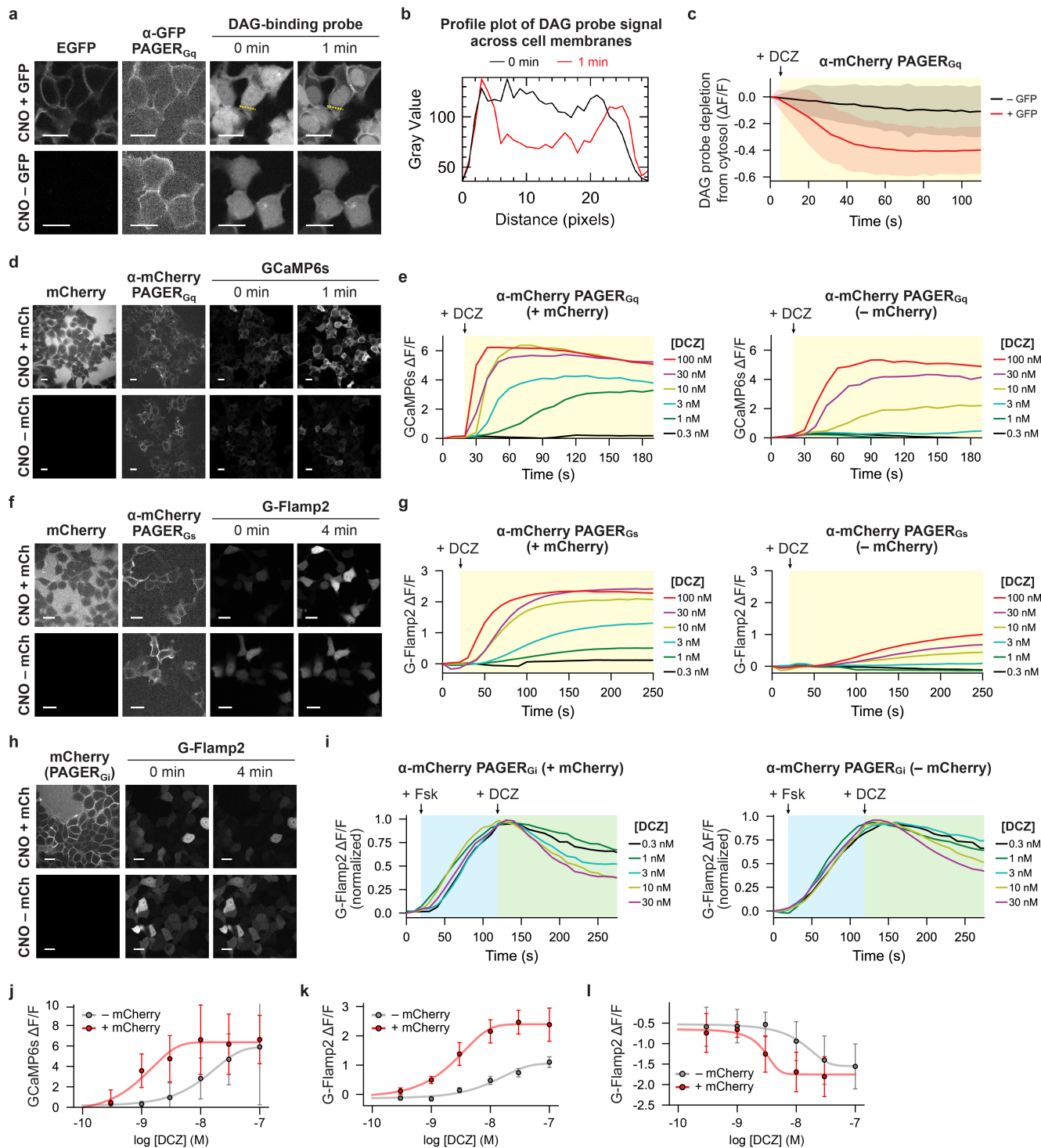
Extended Data Fig. 7 | Screening muscarinic toxins in PAGER_C for conditional auto-inhibition. **a**, Overlay of muscarinic toxins that have experimentally-solved structures (PDB accession code: MT1, 4DO8; MT2, 1FF4; MT7, 6WJC; MT α , 7ULS). **b**, Schematic of TRUPATH BRET assay used to screen PAGER_C constructs containing various muscarinic toxins (MTs). 1 μ M recombinant TEV protease (TEVp) was added for 90 min prior to CNO addition to relieve auto-inhibition. **c**, Results of TRUPATH screen, showing EC₅₀ values for CNO, with and without TEVp pre-treatment. The rMID-based PAGER_C have ICL2-3 from rM3D grafted into hMIDq. The constructs colored red showed the best dynamic range and were selected as the final PAGER_C's. Full CNO dose-response curves

for all constructs are shown in Supplementary Fig. 6. **d**, Schematic of SPARK-type¹⁵ transcriptional assay used to screen different PAGER_C scaffolds. HEK cells expressing the indicated variant were treated with 1 μ M GFP and 10 μ M CNO for 15 min. 8 h later, luciferase reporter expression was quantified. **e**, Summary of SPARK screening results, showing that MT1 toxin was best for gating PAGER_{Gq}, and MT3 toxin was best for gating PAGER_{G_i}, in agreement with the data from the TRUPATH assay (b-c). Plots are mean \pm s.d. for 3 technical replicates per condition, $n = 1$ independent experiment. p -values were determined using two-tailed Student's t tests. *, $p < 0.05$; ***, $p < 0.001$.



Extended Data Fig. 8 | Domain structures and characterization of PAGER_c.
a, Domain structures of optimized PAGER_{Gq}, PAGER_{Gs}, PAGER_{Gi}, and PAGER_{G12}. The W442A mutation was found to improve membrane localization of M1 DREADD by reducing constitutive receptor internalization (Uwada et al., *J Cell Sci*, 2014) and thus introduced to both PAGER_{Gq} and PAGER_{G12}. **b**, Immunofluorescence staining of HEK293 T cells stably expressing PAGER_c's, using α-ALFA-Alexa Fluor 647 (PAGER; green) and DAPI (nuclear stain; blue). Images are representative

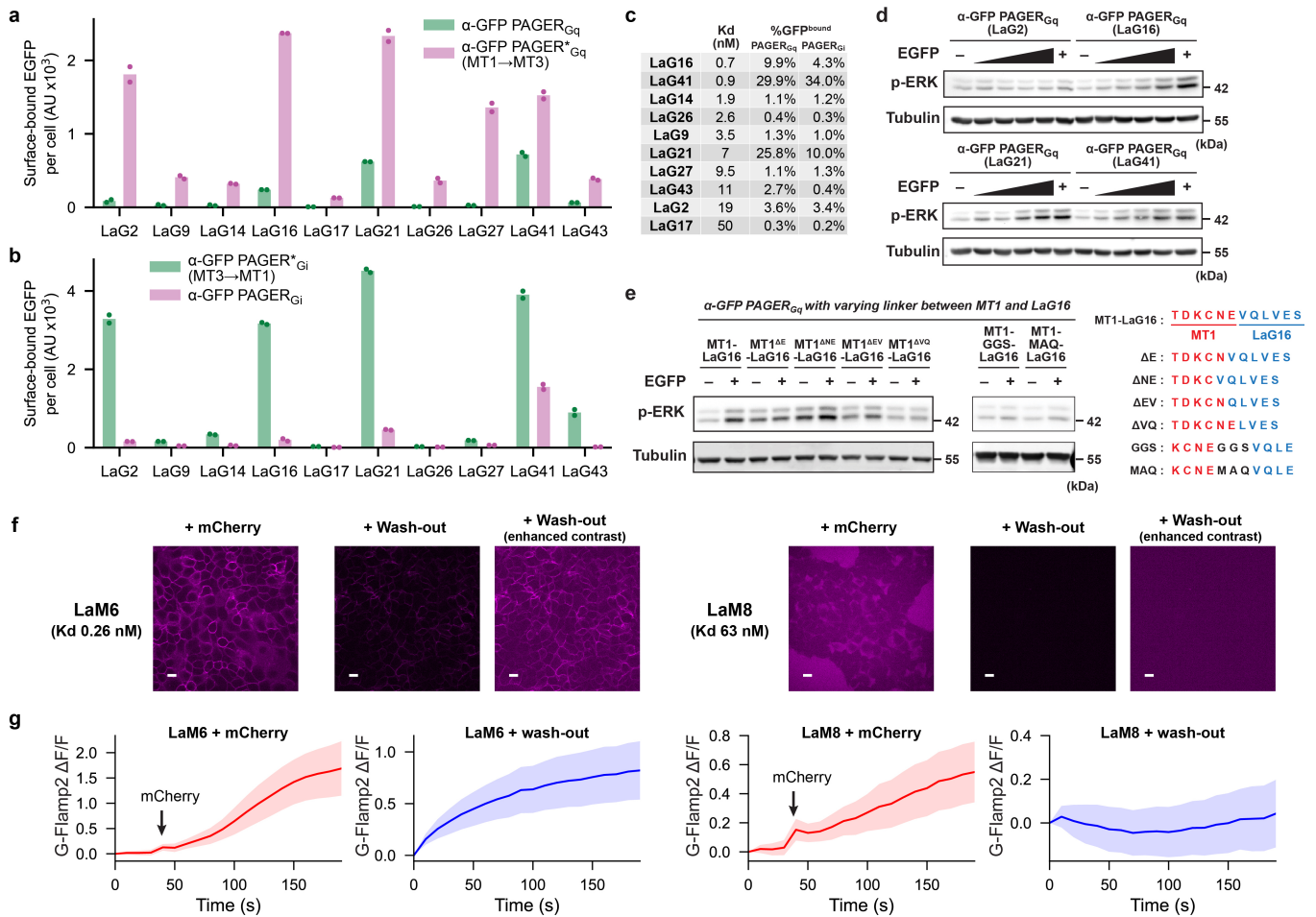
of $n = 2$ independent experiments. Scale bars, 20 μm . **c**, Raw BRET data from TRUPATH assay shown in Fig. 3i-l. Plots are mean \pm s.d. (3 technical replicates per condition, representing $n = 4$ independent experiments). **d**, Testing cross-activation in each TRUPATH assay by all four PAGER_c's. Plots are mean \pm s.d. for 3 technical replicates per condition, $n = 1$ independent experiment. **e**, Raw BRET values for data in (d).



Extended Data Fig. 9 | Antigen-gated control of second messengers by PAGER_c.

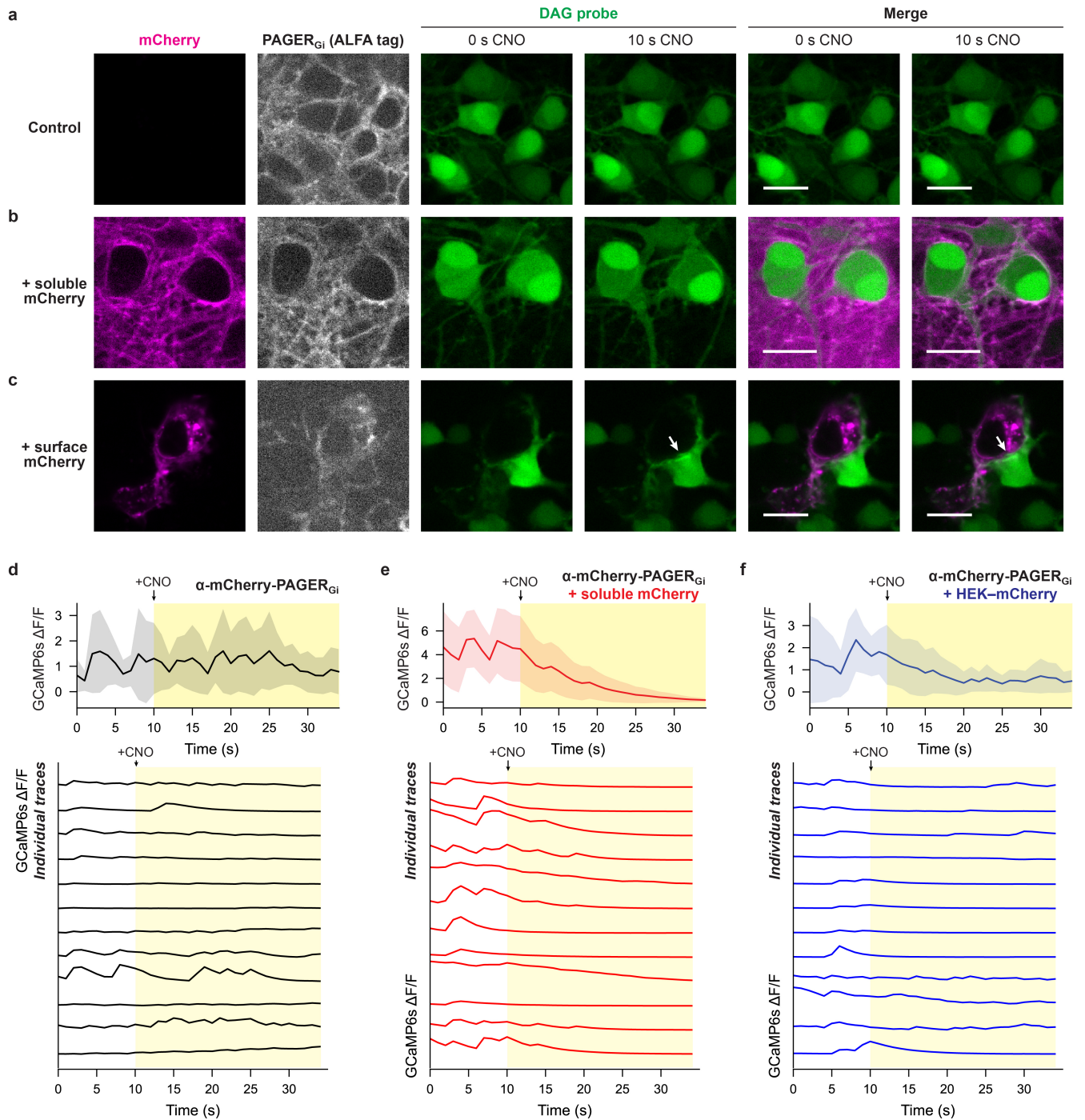
a, Representative images showing antigen-dependent control of endogenous DAG lipid production with PAGER_{Gq}. HEK cells expressing α -GFP PAGER_{Gq} and DAG probe were treated with 1 μ M GFP and 100 nM CNO and imaged over time. **b**, Representative profile plot of DAG probe signal across cell membranes (marked by yellow dashed line in (a)), at $t = 0$ min (black) and $t = 1$ min (red). **c**, Time-course plot of experiment in (a). Plots show mean \pm s.d. for 28 and 27 individual cells, respectively, examined over $n = 3$ independent samples. **d**, Representative images showing antigen-dependent control of cytosolic Ca²⁺ with PAGER_{Gq}. HEK cells expressing α -mCherry PAGER_{Gq} and GCaMP6s were preincubated with 2 μ M mCherry for 3 min, stimulated with 100 nM CNO and imaged over time. **e**, Time-course plots of experiment in (d) at several different DCZ concentrations. **f**, Representative images showing

antigen-dependent control of cytosolic cAMP with PAGER_{Gs}. HEK cells expressing α -mCherry PAGER_{Gs} and G-Flamp2³³ reporter were preincubated with 2 μ M mCherry for 3 min, stimulated with 100 nM CNO and imaged over time. **g**, Time-course plots of experiment in (f) at several different DCZ concentrations. **h**, Representative images showing antigen-dependent control of cytosolic cAMP with PAGER_{Gs}. HEK cells expressing α -mCherry PAGER_{Gs} and G-Flamp2 reporter were preincubated with 2 μ M mCherry for 3 min and stimulated with 2 μ M forskolin (Fsk) for 100 seconds before addition of 25 nM CNO. **i**, Time-course plots of experiment in (h) at several different DCZ concentrations. Plots in (e, g, i) show mean from 50 cells, representing $n = 3$ independent experiments. **j**–**l**, DCZ dose-response curves generated from data in (e, g, i). Plots are mean \pm s.d. for 50 cells, representing $n = 3$ independent experiments. All scale bars, 20 μ m.



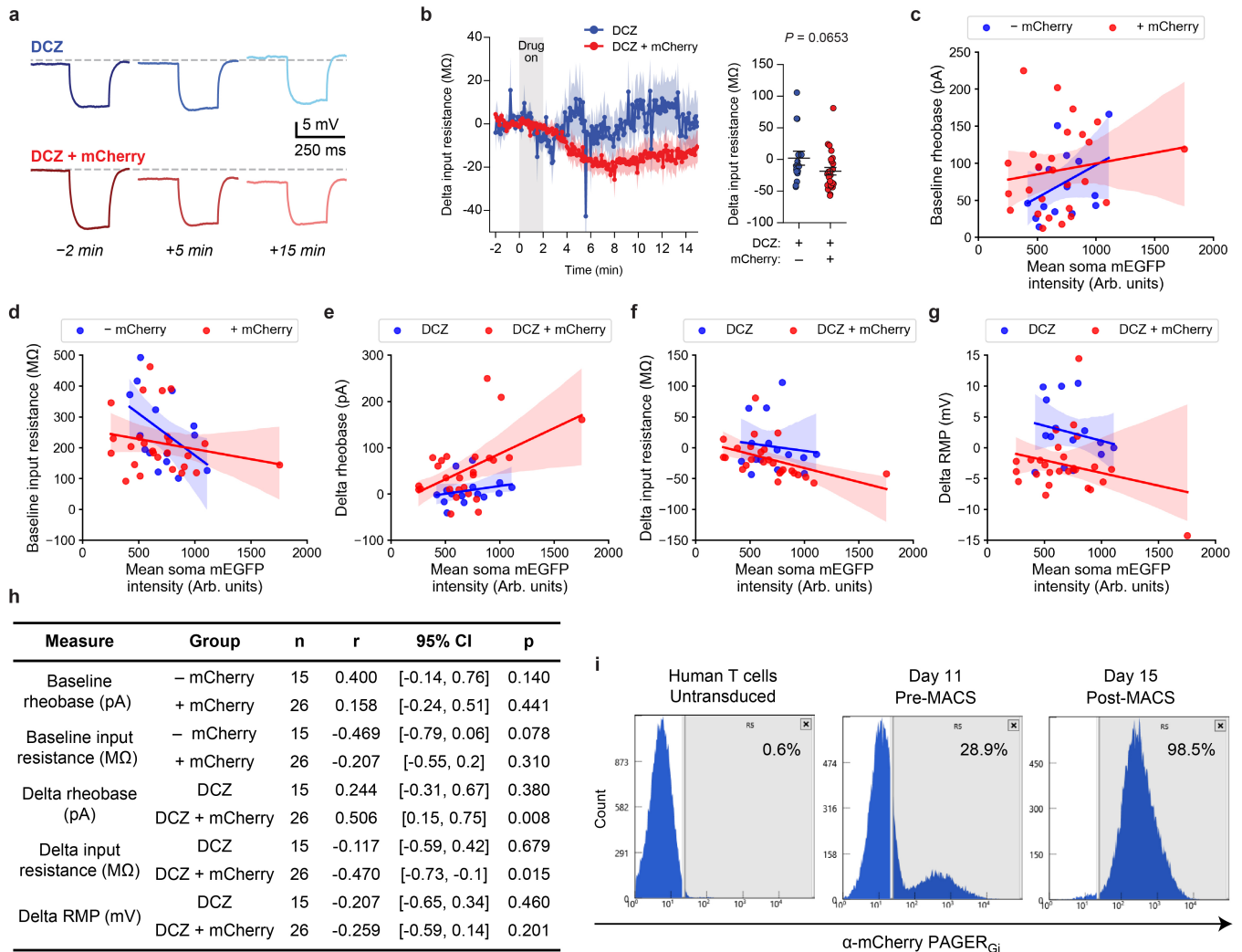
Extended Data Fig. 10 | Evaluation of different nanobodies and toxin truncations in PAGER_{Gq}. **a**, Varying GFP nanobodies in original α -GFP PAGER_{Gq} (MT1-LaGx-hM1Dq; green) or in α -GFP PAGER_{Gq}* (MT3-LaGx-hM1Dq; magenta) where MT1 autoinhibitory domain was swapped with MT3 toxin. MT1 has higher reported affinity to M1 receptor than MT3. HEK cells expressing PAGER_{Gq} with the indicated nanobody were treated with 10 μ M GFP for 15 min, washed, and then analyzed by FACS. Quantitation was based on the average GFP signal per cell. Data representative of $n = 2$ biologically independent samples. **b**, Same assay as (a) but with α -GFP PAGER_{Gi}* (MT1-LaGx-hM4Di; green) and α -GFP PAGER_{Gi} (MT3-LaGx-hM4Di; magenta). MT3 has higher reported affinity to M4 receptor than MT1. Data representative of $n = 2$ biologically independent samples. **c**, Table summarizing reported affinities (K_d) of α -GFP nanobodies along with the amount of GFP bound onto PAGER_{Gq} (divided by the maximum amount of GFP bound in the lack of any antagonism). **d**, Western blots showing phosphorylation of endogenous ERK in response to GFP and CNO activation of PAGER_{Gq} with four different GFP nanobodies. HEK cells expressing the indicated

α -GFP PAGER_{Gq} were stimulated with 100 nM CNO and 0, 0.5, 5, 50, 500, or 5000 μ M antigen for 3 min, before cell lysis and analysis. Phospho-ERK increase started becoming apparent at 50 nM antigen. Similar results were obtained in two independent experiments. **e**, Similar assay as (d) with 1 μ M antigen, but using PAGER_{Gq} variants containing toxin truncations or linkers between MT1 and nanobody. Truncations or linker sequences of the variants used are shown on the right. Similar results were obtained in two independent experiments. **f**, HEK cells co-expressing G-Flamp2 and α -mCherry PAGER_{Gs} with LaM6 (high affinity; K_d 0.26 nM) or LaM8 (low affinity; K_d 63 nM) nanobody were preincubated in 3 nM DCZ and imaged over time, and 1 μ M mCherry was added at $t = 30$ s (red plots). After 3 min, cells were washed with 3 nM DCZ for three times and imaged over time (blue plots). Plots are mean \pm s.d. for 50 cells, representing $n = 2$ independent experiments. **g**, Representative images showing mCherry bound to HEK cells. Left images (+mCherry) were obtained 3 min after mCherry addition, and right images (+Wash-out) were obtained after washing cells with 3 nM DCZ three times. Scale bars, 20 μ m.



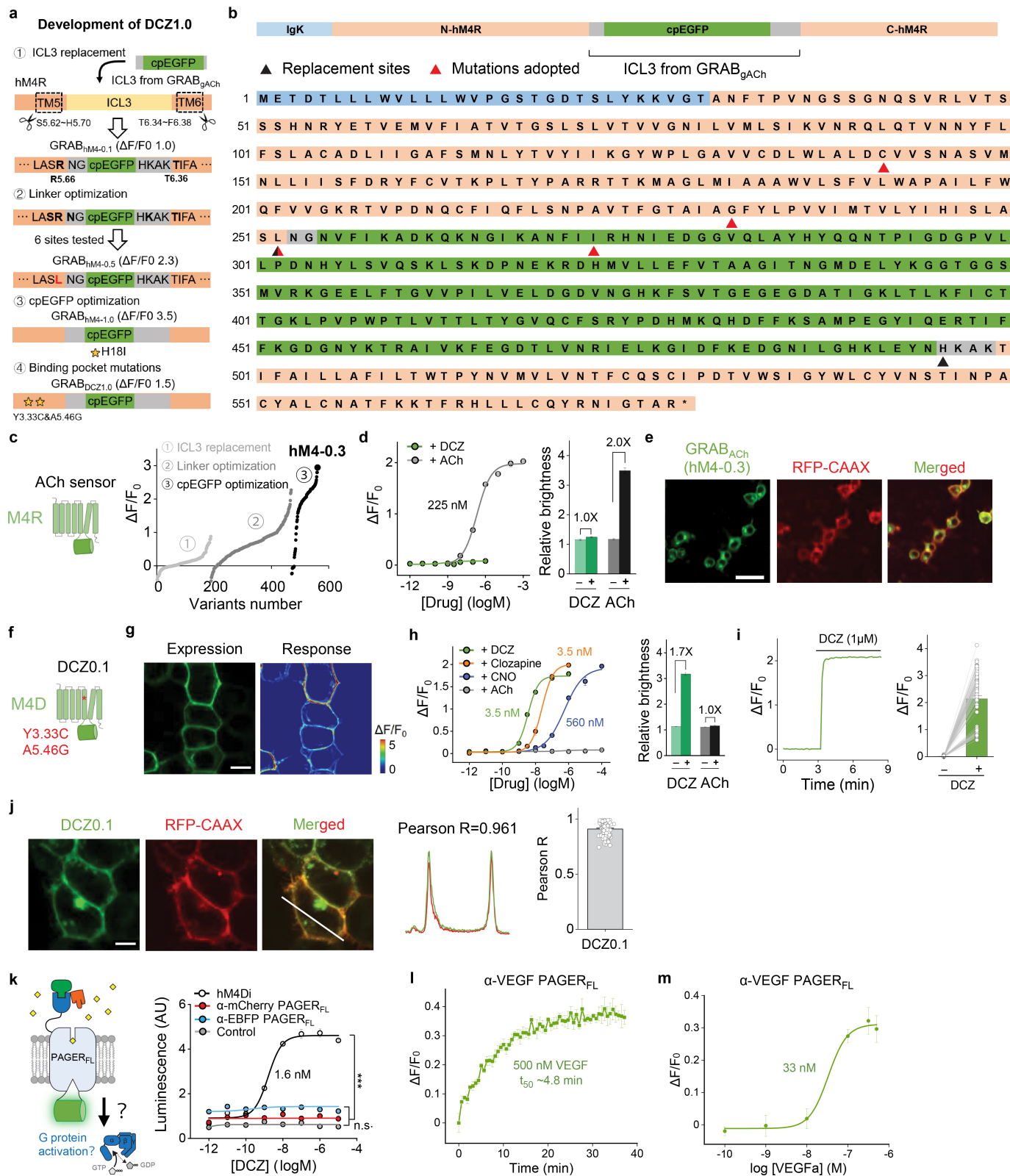
Extended Data Fig. 11 | PAGER_{Gi} mediates antigen-dependent control of neuronal activity in culture. **a–c**, Representative images of antigen-gated DAG production in neurons. Rat cortical neurons expressing α-mCherry PAGER_{Gi} and DAG probe (C1_{PKCY}-mCherry³¹) were stimulated with 100 nM CNO and imaged over time. In (b), neurons were preincubated with 1 μM mCherry (no washout). In (c), HEK cells expressing surface mCherry (pink) were plated on top of neurons. Note the DAG probe accumulation at sites of HEK-neuron contact (arrowheads). Scale bars, 20 μm. Similar results were obtained in three

independent experiments. **d–f**, Calcium traces in rat cortical neurons co-expressing α-mCherry PAGER_{Gi} and GCaMP6s, with no antigen (d), with 1 μM mCherry (e), or co-plated with HEK cells expressing surface mCherry (f). CNO was added at t = 10 s to a final concentration of 30 nM. Plots are mean ± s.d. of $\Delta(F - F_{\text{base}})/F_{\text{base}}$ in GCaMP6s signal (where F_{base} is the minimum signal recorded in the time window) for 12 neurons, representing $n = 2$ independent experiments. This is similar to data presented in Fig. 4a–d but using CNO instead of DCZ.



Extended Data Fig. 12 | PAGER_{Gi} expression in acute brain slices and primary T cells. **a**, Representative traces of voltage responses to -100pA stepwise current injections relative to onset of 2 min bath application of DCZ (100 nM) ± soluble mCherry (1 μM). Dashed line at -65 mV. **b**, Changes in input resistance upon 2-minute DCZ addition. *n* = 15 cells/7 animals DCZ, *n* = 26 cell/6 animals DCZ+mCherry. Plots show mean ± S.E.M. (Mixed linear model regression analysis; *Z* = 1.84, *P* = 0.0653). **c-h**, Correlation between PAGER_{Gi}-associated mEGFP expression and neuronal intrinsic properties. The degree of mEGFP expression, as an indicator of PAGER_{Gi} expression levels in neurons, supports PAGER_{Gi} alone having no impact on baseline rheobase (c) or input resistance (d) properties, including in the presence of soluble mCherry. Construct expression

levels were correlated with the degree of rheobase (e) and input resistance (f) shifts following DCZ+mCherry exposure, but not with DCZ alone. Resting membrane potential (RMP) shifts were not specifically linked to mEGFP expression levels (g). PAGER_{Gi}-associated mEGFP mean signal intensity was measured from widefield images acquired prior to the start of each whole cell recording, within a freehand selection surrounding the soma made in ImageJ. Pearson correlation was used for analyses, as summarized in (h). **i**, Histograms showing percent of human primary T cells expressing α-mCherry PAGER_{Gi} after lentiviral transduction, on Day 11 before MACS enrichment and on Day 15 after MACS enrichment.



Extended Data Fig. 13 | See next page for caption.

Extended Data Fig. 13 | Engineering PAGER_{FL}. **a**, Summary of DCZ1.0 development. DCZ1.0 is the receptor portion of PAGER_{FL}, lacking the nanobody and toxin. Starting from M4R, we ① screened cpEGFP insertion sites within the ICL3 loop in gACh sensor²; ② optimized key residues (shown in bold) in the linkers; and ③ optimized critical residues in cpEGFP. **b**, Sequence of optimized DCZ1.0 sensor. The residues related to ICL3 replacement and mutations incorporated during the optimization process are marked. **c**, Summary of ACh sensor screening and optimization. The number of ACh sensor variants tested during each optimization process is shown in x-axis. The final optimized variant was named hM4-1.0. **d**, Response (left) and relative brightness (right) of hM4-1.0 to various concentrations of ACh and DCZ. *n* = 300 cells from 3 independent experiments. Error bars=S.E.M. **e**, Membrane expression of hM4-1.0 in HEK293T cells. RFP-CAAX is a membrane-targeted RFP. Scale bars, 50 μm. *n* = 3 independent experiments. **f**, DCZ1.0 incorporates the two additional DREADD mutations compared to hM4-1.0. **g**, Representative images of expression and response of DCZ1.0 sensor to 1 μM DCZ. Scale bars, 10 μm. **h**, Drug response curves (left) and relative brightness (right) of DCZ1.0. *n* = 300 cells from 3 independent experiments. Error bars=S.E.M. **i**, Fluorescence time traces (left) showing the rate of EGFP fluorescence onset after 1 μM DCZ addition. Group summary

(right) of $\Delta F/F_0$ with or without DCZ addition. *n* = 126 cells from 3 independent experiments. Error bars=S.E.M. **j**, Example fluorescence images and intensity line scan profiles of DCZ1.0 (green), RFP-CAAX (red), and merged image in the presence of DCZ (1 μM). The white line indicated the ROI for intensity profiling, and the Pearson R was calculated and used to indicate the membrane trafficking index of the sensor. *n* = 112 cells from 3 independent experiments. Error bars=S.E.M. Scale bars, 10 μm. **k**, G protein and coupling were measured using the split-luciferase complementation assay³ in cells expressing α-mCherry PAGER_{FL} (red), α-EBFP PAGER_{FL} (blue) in the presence of the indicated concentrations of DCZ; The DCZ-responsive DREADD hM4Di (black) was used as a positive control and no receptor (grey) was used as a negative control. AU, arbitrary units. *n* = 3 independent experiments. Error bars=S.E.M. (one-way ANOVA with Tukey's multiple comparisons test; *** *p* < 0.005; n.s.=not significant). **l-m**, Response of α-VEGF PAGER_{FL} developed by swapping nanobody with α-VEGF nanobody (Nb35). **l**, Fluorescence time trace showing the rate of EGFP fluorescence onset after VEGF addition. DCZ was present at 100 nM. **m**, Response of α-VEGF PAGER_{FL} to various concentrations of VEGF. DCZ was present at 100 nM. *F*₀ is the intensity of sensors with 100 nM DCZ addition. *n* = 300 cells from 3 independent experiments. Error bars=S.E.M.

Reporting Summary

Nature Portfolio wishes to improve the reproducibility of the work that we publish. This form provides structure for consistency and transparency in reporting. For further information on Nature Portfolio policies, see our [Editorial Policies](#) and the [Editorial Policy Checklist](#).

Statistics

For all statistical analyses, confirm that the following items are present in the figure legend, table legend, main text, or Methods section.

n/a | Confirmed

- The exact sample size (n) for each experimental group/condition, given as a discrete number and unit of measurement
- A statement on whether measurements were taken from distinct samples or whether the same sample was measured repeatedly
- The statistical test(s) used AND whether they are one- or two-sided
Only common tests should be described solely by name; describe more complex techniques in the Methods section.
- A description of all covariates tested
- A description of any assumptions or corrections, such as tests of normality and adjustment for multiple comparisons
- A full description of the statistical parameters including central tendency (e.g. means) or other basic estimates (e.g. regression coefficient) AND variation (e.g. standard deviation) or associated estimates of uncertainty (e.g. confidence intervals)
- For null hypothesis testing, the test statistic (e.g. F , t , r) with confidence intervals, effect sizes, degrees of freedom and P value noted
Give P values as exact values whenever suitable.
- For Bayesian analysis, information on the choice of priors and Markov chain Monte Carlo settings
- For hierarchical and complex designs, identification of the appropriate level for tests and full reporting of outcomes
- Estimates of effect sizes (e.g. Cohen's d , Pearson's r), indicating how they were calculated

Our web collection on [statistics for biologists](#) contains articles on many of the points above.

Software and code

Policy information about [availability of computer code](#)

Data collection

Data analysis

For manuscripts utilizing custom algorithms or software that are central to the research but not yet described in published literature, software must be made available to editors and reviewers. We strongly encourage code deposition in a community repository (e.g. GitHub). See the Nature Portfolio [guidelines for submitting code & software](#) for further information.

Data

Policy information about [availability of data](#)

All manuscripts must include a [data availability statement](#). This statement should provide the following information, where applicable:

- Accession codes, unique identifiers, or web links for publicly available datasets
- A description of any restrictions on data availability
- For clinical datasets or third party data, please ensure that the statement adheres to our [policy](#)

All data supporting the findings of this study are available within the paper and its Supplementary Information. No datasets were generated or analyzed during the current study.

Research involving human participants, their data, or biological material

Policy information about studies with [human participants or human data](#). See also policy information about [sex, gender \(identity/presentation\), and sexual orientation](#) and [race, ethnicity and racism](#).

Reporting on sex and gender	N/A
Reporting on race, ethnicity, or other socially relevant groupings	N/A
Population characteristics	N/A
Recruitment	N/A
Ethics oversight	N/A

Note that full information on the approval of the study protocol must also be provided in the manuscript.

Field-specific reporting

Please select the one below that is the best fit for your research. If you are not sure, read the appropriate sections before making your selection.

Life sciences Behavioural & social sciences Ecological, evolutionary & environmental sciences

For a reference copy of the document with all sections, see nature.com/documents/nr-reporting-summary-flat.pdf

Life sciences study design

All studies must disclose on these points even when the disclosure is negative.

Sample size	No statistical method was used to predetermine sample size. Sample sizes were determined based on at least three independent experiments and based on accepted practices as provided in the literature and appropriately cited. Based on previous studies in the field, sample sizes in this study enable statistical analysis and ensure reproducibility.
Data exclusions	No data was excluded from the analyses.
Replication	All experimental findings presented in this study were reproducible based on independent replicate measurements as described in detail in the methods section and the corresponding figure legends.
Randomization	Randomization as would be performed with human samples or animal studies does not apply to this study.
Blinding	Blinding as would be performed with human samples or animal studies does not apply to this study.

Reporting for specific materials, systems and methods

We require information from authors about some types of materials, experimental systems and methods used in many studies. Here, indicate whether each material, system or method listed is relevant to your study. If you are not sure if a list item applies to your research, read the appropriate section before selecting a response.

Materials & experimental systems

n/a	Involved in the study
<input type="checkbox"/>	<input checked="" type="checkbox"/> Antibodies
<input type="checkbox"/>	<input checked="" type="checkbox"/> Eukaryotic cell lines
<input checked="" type="checkbox"/>	<input type="checkbox"/> Palaeontology and archaeology
<input type="checkbox"/>	<input checked="" type="checkbox"/> Animals and other organisms
<input checked="" type="checkbox"/>	<input type="checkbox"/> Clinical data
<input checked="" type="checkbox"/>	<input type="checkbox"/> Dual use research of concern
<input checked="" type="checkbox"/>	<input type="checkbox"/> Plants

Methods

n/a	Involved in the study
<input checked="" type="checkbox"/>	<input type="checkbox"/> ChIP-seq
<input checked="" type="checkbox"/>	<input type="checkbox"/> Flow cytometry
<input checked="" type="checkbox"/>	<input type="checkbox"/> MRI-based neuroimaging

Antibodies

Antibodies used	Phospho-p44/42 MAPK (phospho-Erk1/2; Cell Signaling Technology #9101), p44/42 MAPK (Erk1/2; Cell Signaling Technology #9107),
-----------------	---

Antibodies used	and β -Tubulin (Cell Signaling Technology #86298).
Validation	All antibodies used in this study were recommended on manufacturer's website for use in the employed application. Relevant citations can be found at the web page for each antibody (https://www.cellsignal.com/products/primary-antibodies/phospho-p44-42-mapk-erk1-2-thr202-tyr204-antibody/9101 , https://www.cellsignal.com/products/primary-antibodies/p44-42-mapk-erk1-2-3a7-mouse-mab/9107 , and https://www.cellsignal.com/products/primary-antibodies/b-tubulin-d3u1w-mouse-mab/86298?site-search-type=Products&N=4294960093+102236+4294967092+4294956287&Ntt=tubulin&fromPage=plp , respectively).

Eukaryotic cell lines

Policy information about [cell lines and Sex and Gender in Research](#)

Cell line source(s)	HEK293T (ACC), Primary cortical neurons from rat embryos
Authentication	No separate authentication beyond that provided with source.
Mycoplasma contamination	Cells test negative for mycoplasma.
Commonly misidentified lines (See ICLAC register)	None.

Animals and other research organisms

Policy information about [studies involving animals; ARRIVE guidelines](#) recommended for reporting animal research, and [Sex and Gender in Research](#)

Laboratory animals	Adult female C57BL/6 mice (Jackson Laboratory) 4-8 weeks old were used.
Wild animals	N/A
Reporting on sex	Sex was not considered in the study design. Only female mice were used.
Field-collected samples	N/A
Ethics oversight	Administrative Panel on Laboratory Animal Care of Stanford University (Protocol #30183)

Note that full information on the approval of the study protocol must also be provided in the manuscript.

Plants

Seed stocks	N/A
Novel plant genotypes	N/A
Authentication	N/A